6

Biomechanical Analysis of Restored Teeth with Cast Intra-Radicular Retainer with and Without Ferrule

Isis Andréa Venturini Pola Poiate[1],
Edgard Poiate Junior[2] and Rafael Yagöe Ballester[3]
[1]*Federal Fluminense University,*
[2]*Pontifical Catholic University,*
[3]*University of São Paulo,*
Brazil

1. Introduction

For the prosthetic reconstruction of endodontically treated teeth with large loss of tooth structure a lot of times become indispensable to obtain retention by the use of post and core systems. The retention loss and the dental fractures are the two failures more commonly described in this restoration type (Ferrari & Mannocci, 2000).

The dental fracture tends to happen longitudinally with the end below the alveolar bone crest, what constitutes a no restorative failure and leads to the tooth's loss. This failure type is attributed mainly to the use of posts with length and/or diameter incorrect and deficiencies in dental structure preservation[1].

The intra-radicular post is used to provide retention to a core, but would also have the function of distributing the functional load in a larger area of the remaining coronary structure and dental root. However, many authors (Assif & Gofil, 1994; Martinez-Insua et al., 1999; Rundquist & Versluis, 2006; Whitworth et al., 2002) have been demonstrating that this reconstruction method doesn't restore the original strength of a vital tooth, what is attributed to the wedge effect that this restoration type causes and to the stiffness difference between the post and the tooth.

This effect appears when the load induces the post intrusion inside the dental root. When being pushed, the wedge tends to increase the perimeter of the remnant transversal section due to the tensile stress guided parallel to the circular outlines of the tooth's transversal section. These tangent stresses can cause vertical fracture (Rundquist & Versluis, 2006).

An attempt to increase the root strength front to the physiologic load is the ferrule making that is a metallic necklace of 360° that surrounds the axial walls of the remnant dentine and can be propitiated by the core or by the crown, and tends to produce the encirclement of the root. This "ferrule effect" would protect the pulpless tooth against fracture by counteracting spreading forces generated by the post. The core should extend apical to the shoulder of the

preparation to provide a 1.5 to 3.0 mm ferrule of the intact tooth structure (Tan et al., 2005; Pereira et al., 2006; Morgano, 1996; Morgano & Bracket, 1999).

According to Loney et al (1990), the ferrule supplied by the core contributes for the most balanced stress distribution in the dental root and it could compress the remnant structure.

The understanding of the biomechanical principles and restorations applicability is important to design restorations to provide larger strength and retention. The aim of this study was to evaluate the ferrule geometry formed by core on the stress developed in the dental root when a second superior premolar is submitted to four different load conditions.

2. Materials and methods

A natural healthy tooth model (H) was generated in the MSC/PATRAN 2005 (MSC Software Corporation, Santa Ana, CA, USA). On that model modifications were accomplished for the creation of five new models with retainer intra-radicular.

The 3D model of the maxillary second premolar was built based on data presented by Shillinburg & Grace (1973), regarding the measures of the dentin thickness in the mesio-distal and vestibular-lingual axis in four horizontal slices (with 3.5 mm interval) accomplished along the main axis of the dental root starting from the cementoenamel junction. The dentin's thickness in the remnant of the root was built by the interpolation with a spline curve starting from the existent data, following the root anatomy. The pulp dimensions were built based on the data presented by Green & Brooklyn (1960), that it supplies the average diameter of the apical foramen and Shillinburg & Grace (1973), that it supplies the average dimensions in the cervical area.

For the making of the crown geometry the enamel thickness and coronary dentin were based on the data presented by Shillinburg & Grace (1973), through slices of interval of 1 mm, by Cantisano at al. (1987) and Ueti at al. (1997). The height of the vestibular cusp was considered larger than the lingual cusp in 0.9 mm (Shillinburg et al., 1972).

The lamina dura was represented with mechanical properties equal of the cortical bone and as a uniform layer of 0.25 mm thickness as well as the periodontal ligament (Lee et al., 2000).

The models that represented intra-radicular retainer were built from the natural healthy tooth model already. Specify modifications were accomplished in the area corresponding to the pulp and to the dentin, in the places corresponding to the core and porcelain-faced crown.

The dimension of the pulp was enlarged to reproduce the endodontic access stage (Cohen & Hargreaves 2005), the biomechanical prepare and the filling of the root canal.

The porcelain-faced crown was represented with the same outline of the enamel, being average thickness of 1.5 mm in the vestibular face, 1.2 mm in the lingual face, 1.0 mm in the proximal face and 2.0 mm in the occlusal face, with an end in chamfer around the core. The minimum thickness of the metal (NiCr) in the restoration porcelain-faced was 0.3 mm (Yamamoto, 1985).

The zinc phosphate cement was select because is usually used for cementation of the crown and of intra-radicular retainer with thickness from 50 to 100 μm (Anusavice, 2003) and the gutta-percha height was of 5 mm (Morgano, 1996).

In four models with intra-radicular retainer was varied the ending line of the core preparation (with ferrule geometry given by the core) and another model was simulated with simple core (without ferrule), staying the same coronary restoration.

The width and the height of the ferrule were determined as a proportion of the thickness of radicular dentine found in the cementoenamel junction region on the lingual side (1.85 mm), separated for three thirds. For other words, the ferrule with x height varying of 0.62 x 0.62 (T1H1), 0.62 x 1.34 (T1H2), 1.34 x 0.62 (T2H1) and 1.34 x 1.34 mm (T2H2), (Fig. 1).

All of the models with intra-radicular retainer presented the same characteristics in relation to the supporting structures, porcelain-faced crown, cement thickness and apical seal (Fig. 2).

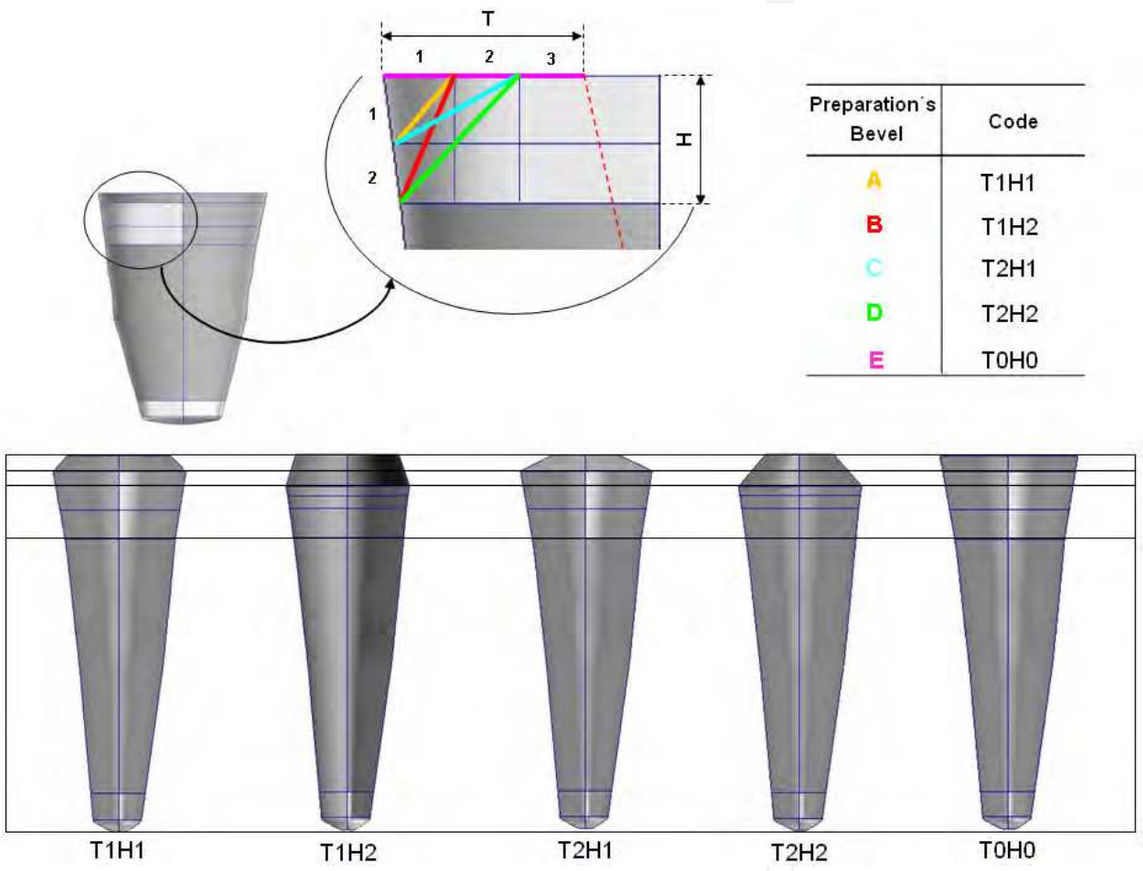

Fig. 1. Ferrule geometries of the radicular dentine in a premolar root.

With the measures of the thickness in each one of the structures (pulp, dentin, enamel) in each face (mesial, distal, lingual, vestibular) a coordinates system was generated with the origin in the pulpal apex and all the values of thickness of the structures were transformed in coordinates. As many coordinates existed to generate the points in the Finite Element (FE) program, a routine in PCL (Patran Command Language) was created to read the spreadsheet and to generate the points. After the points generation (Fig. 3a), the curves were generated and, soon afterwards, the surfaces. Starting from the dental structures surfaces built, the superficial meshes were generated with triangular linear elements (Tri3). After

that, volumetric meshes (Fig. 3d) with tetrahedral linear elements (Tet4) were generated, following the procedures in Poiate et al. (2008, 2009a, 2009b, 2011).

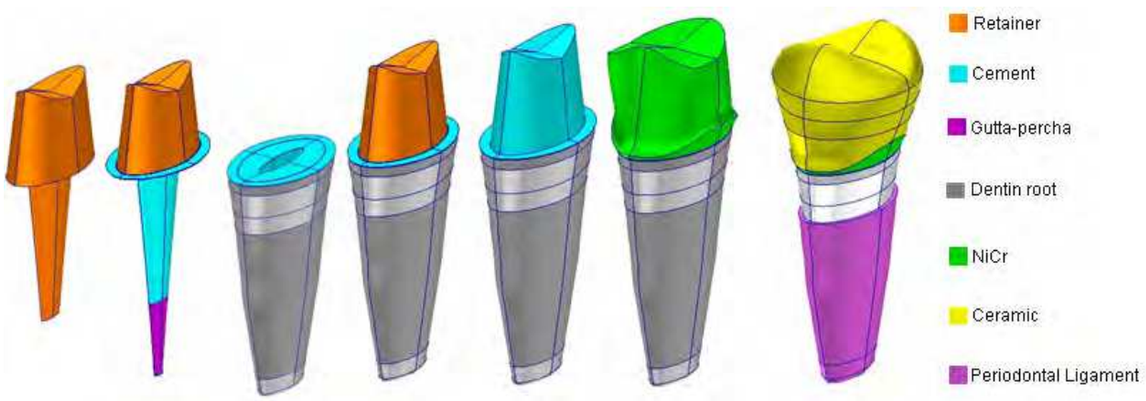

Fig. 2. Structures of the models with intra-radicular retainer.

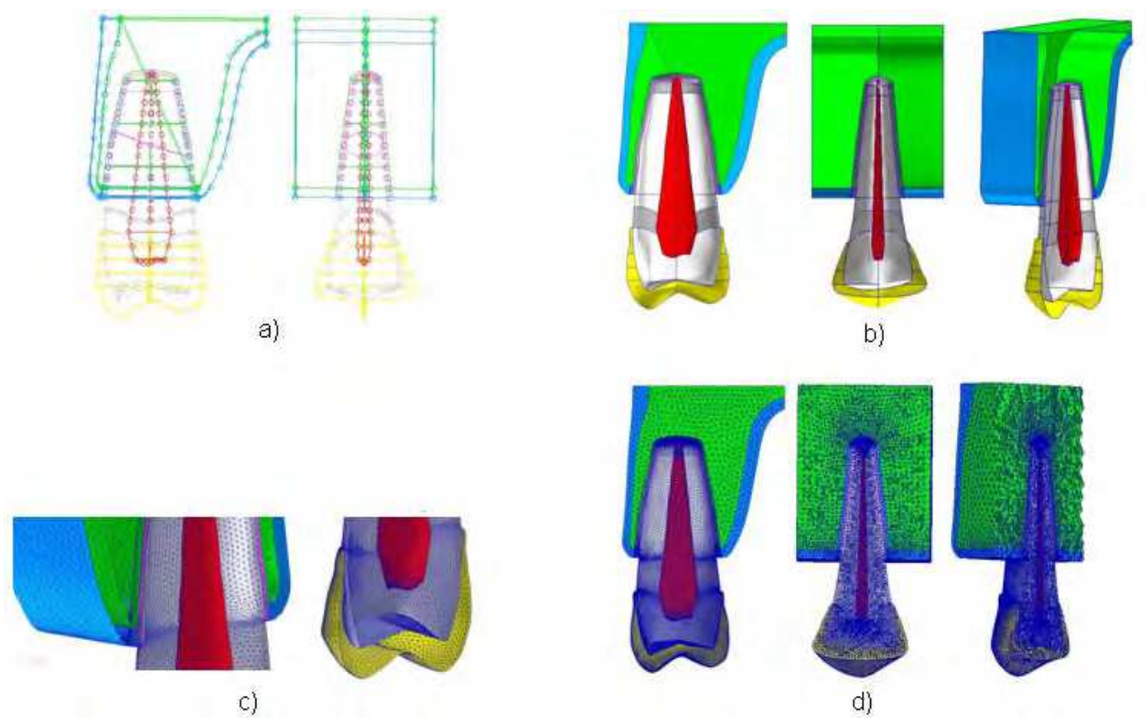

Fig. 3. Sequence of procedures for 3D natural healthy tooth model generation, points generation, dental structures surfaces, superficial and volumetric mesh, respectively.

The degree of discretization of the FE models (Table 1) was established from convergence studies of the results in computer modeling (Pentium 4 3.2 GHz computer with 2.0 Gb RAM memory) to ensure that a proper FE model mesh density was generated and in this way model a realistically anatomic geometry.

Code	Ferrule Thickness x Height	Number of nodes	Number of elements
H	Natural healthy tooth	179403	1109929
T1H1	1 x 1	193034	1226486
T1H2	1 x 2	179430	1142542
T2H1	2 x 1	189438	1200778
T2H2	2 x 2	180720	1148853
T0H0	0 x 0	184750	1175175

Table 1. Models and mesh size.

It was assumed that all the structures in the models were, homogeneous, isotropic and linearly elastic behavior as characterized by two physical properties: Young´s Modulus (E) and Poisson's Ratio (ν), Table 2. The interfaces between the structures were presumed to be perfectly united, because the aim was to provide a comparison of our approach, that this simplification was justified.

Structure / Material	Young´s Modulus (GPa)	Poisson´s Ratio	Reference
Pulp	0.02	0.45	Farah & Craig (1974)
Dentin	18.60	0.31	Ko et al. (1992)
Enamel	41.00	0.30	Ko et al. (1992)
Periodontal ligament	0.0689	0.45	Weinstein et al. (1980)
Cortical bone	13.70	0.30	Ko et al. (1992)
Spongy bone	1.37	0.30	Ko et al. (1992)
Gutta-percha	0.00069	0.45	Friedman et al.(1975)
NiCr	188.00	0.33	Black & Hastings (1998)
Phosphate of Zinc Cement	13.00	0.35	Powers at al. (1976)
Feldspathic Ceramic	82.80	0.35	Peyton & Craig (1963)
Cast radicular retainer (ILOR56: gold-alloy post)	93.00	0.33	Pegoretti et al. (2002)

Table 2. Physical properties of the anatomical structures and materials.

Finally, boundary conditions or the model constraint and the loads are also applied. The constraint conditions applied were: in the maxillary sinus, translation in x, y and z directions and rotations in x, y and z axis, fully anchor; in the mesial and distal extremities of the cortical and spongy bone, translation in x direction (perpendicular to this faces) and rotations in y and z axis were anchor. Four load cases were built varying the site, inclination and the application area of a 291.36 N total static load, maximum masticatory force (Ferrario et al., 2004).

Initially, all of the models received the resultant load intensity of 291.36 N parallel to the tooth's long axis, with the aim to evaluate the wedge effect (Fig. 4). The load was applied on the lingual and vestibular cusp above the occlusal surface, at 45º in relation to the tooth's long axis (Holmes et al. 1996), distributed in 19 nodal points of 0.85 mm² area in vestibular cusp and in 19 nodal points of 0.75 mm² area of in lingual cusp (Kumugai et al., 1999).

After that, the model with ferrule that best minimized the wedge effect, as well as the models that represent natural healthy tooth and restored with simple core (T0H0, without ferrule, Fig. 1) were submitted to the following loads (Fig. 4):

a. Oblique Load with 45º in relation to the tooth's long axis distributed in 19 nodal points of 0.85 mm² area in the vestibular cusp, with the aim to evaluate the vestibular lever effect;
b. Load parallel to the tooth's long axis distributed in 19 nodal points of 0.80 mm² area in the mesial marginal ridge, with the aim to evaluate the proximal lever effect;
c. Oblique Load with 45º in relation to the tooth's long axis pointed to vestibular cusp, distributed in 19 nodal points of 0.80 mm² area in the mesial marginal ridge, with the aim to evaluate the torsion effect.

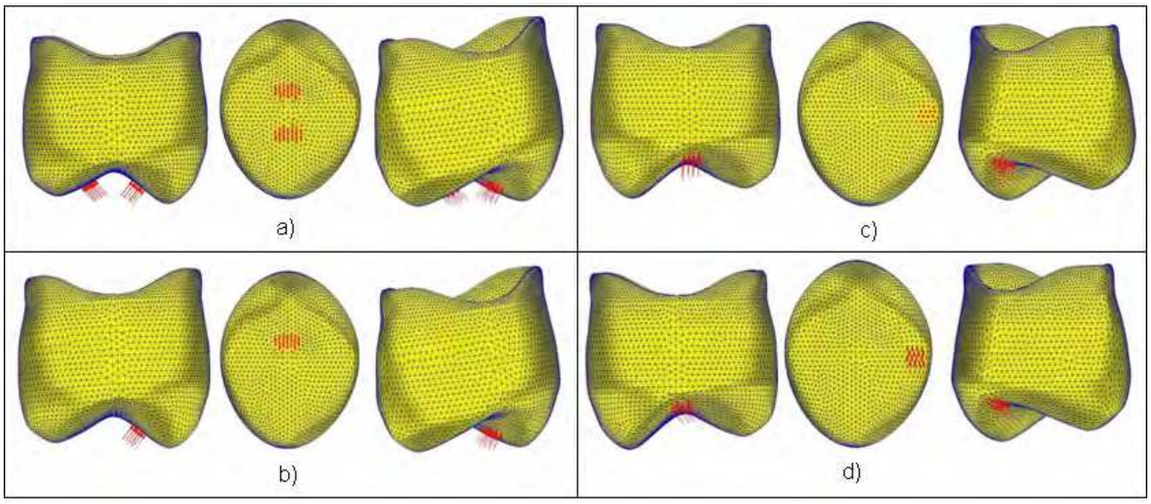

Fig. 4. Place, area and orientation of the load application, a)wedge effect, b)vestibular lever effect, c)proximal lever effect and d)torsion effect.

The processing stage or the solution analysis was performed using MSC/NASTRAN 2005 software (MSC Software Corporation, Santa Ana, CA, USA). The MSC/PATRAN 2005 software, used in the pre-processing, was also used for the post-processing, visualization, and evaluation of the results.

In this study, the maximum principal stress was used as the stress criterion to present the stress patterns distribution in the analyzed models. The cement and dentin's tensile strength of 8.3 MPa (Powers at al., 1976) and 103 MPa (Tanaka et al., 2003), respectively, as well as dentin´s compressive strength of 282 MPa (Tanaka et al., 2003), respectively, will serve as reference for results comparison to evaluate if the loads would be potentially harmful to the studied structures.

3. Results

3.1 Wedge effect

Under load with parallel resultant to the long axis, all of the models answered equally. The differences were just in the dentin area in contact with the ferrule (Fig. 5). The results

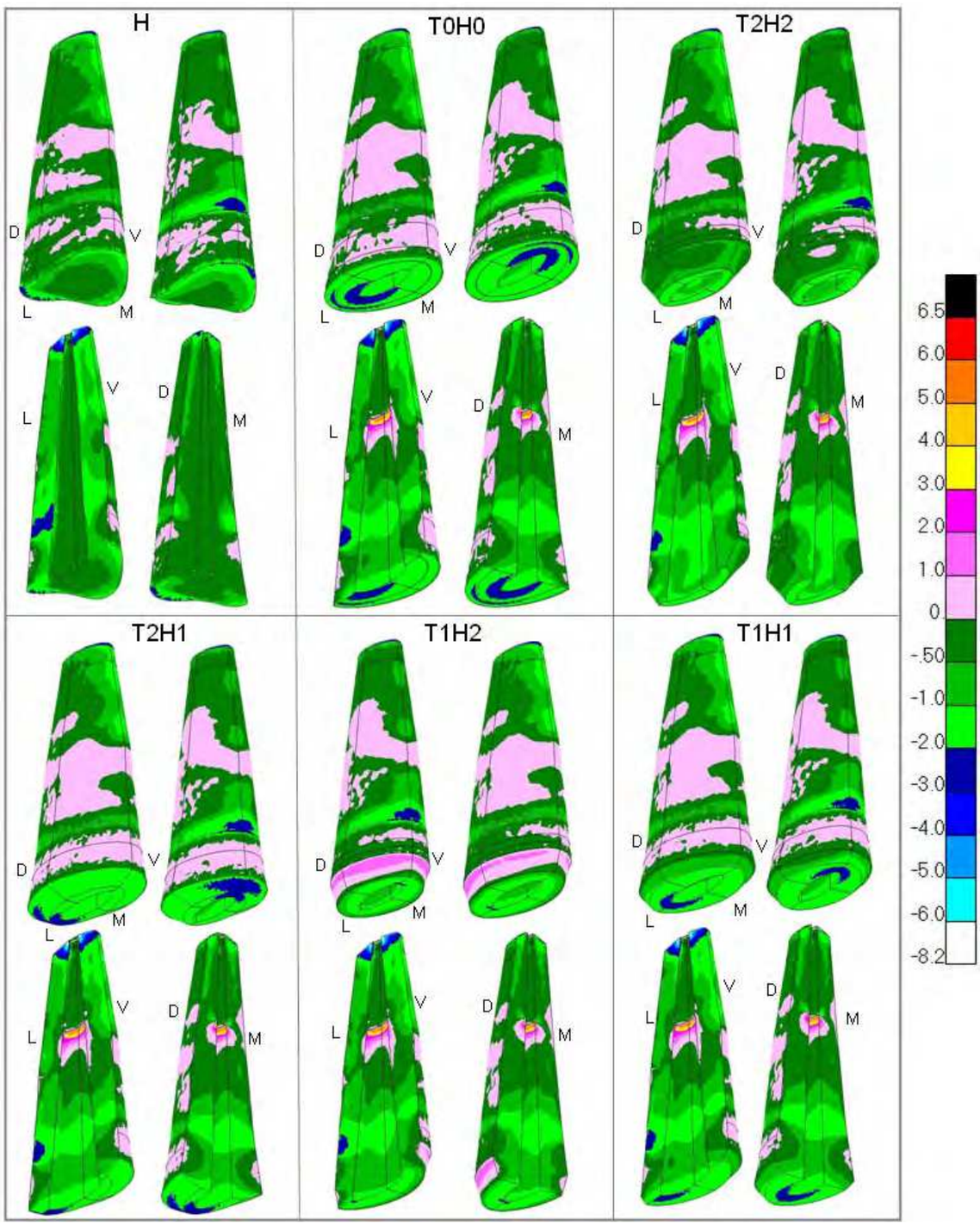

Fig. 5. MPS in all models loaded longitudinally with Vestibular (V)-Lingual (L) and Mesial (M)–Distal (D) slices.

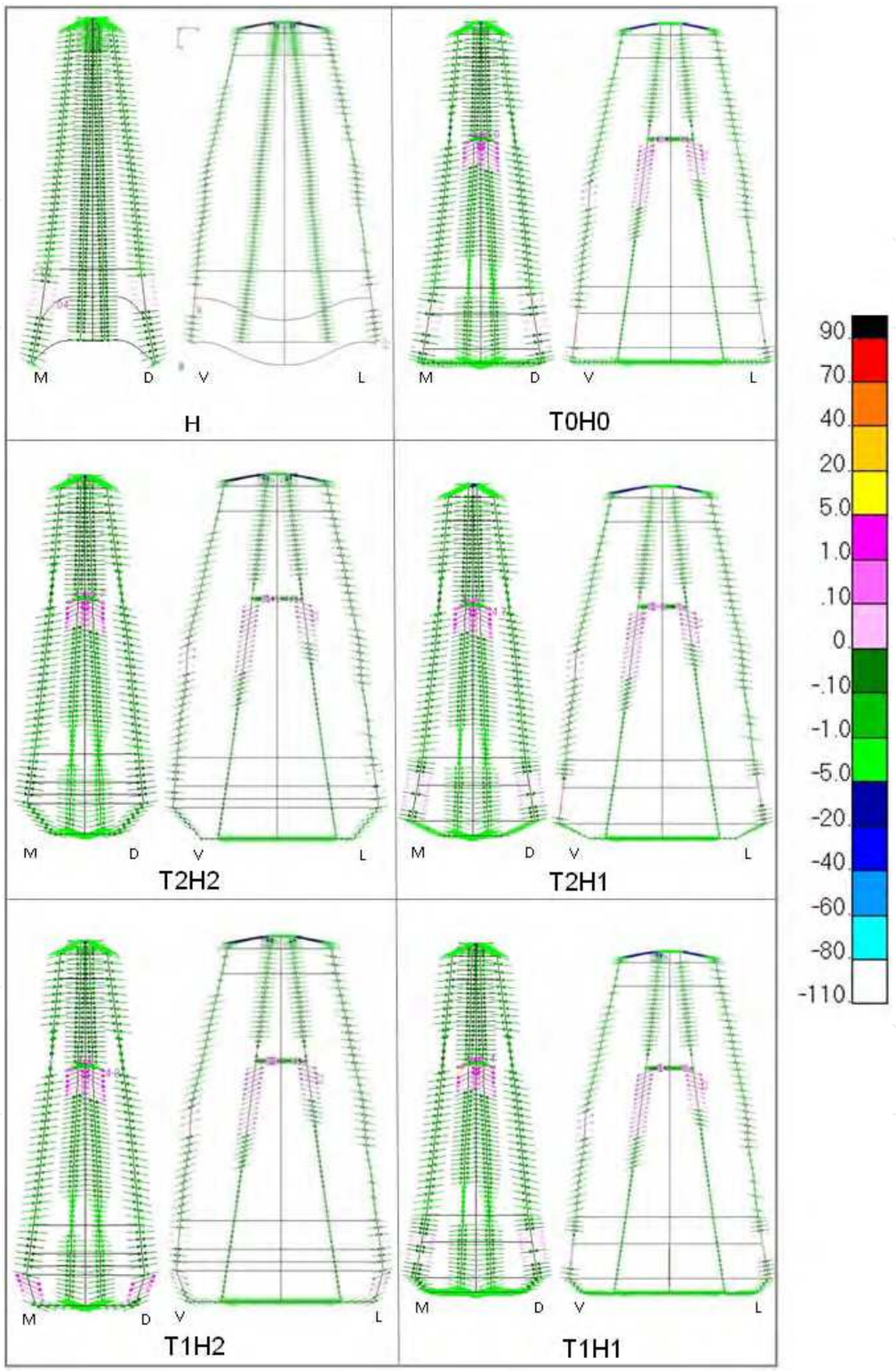

Fig. 6. MPS vectors in the surfaces of the radicular dentine in the wedge effect in M-D and V-L slices.

obtained with models T1H1 and T2H1 presented similar pattern of stress distribution in Maximum Principal Stress (MPS), but different from models T1H2 and T2H2 (that present low tensile stress under the ferrule). In the model H, the dentin area between the bone and the enamel presents some tensile stress, but the Fig. 6 show that the stress vector direction is not totally tangential to the transversal section and it wouldn't be deleterious, nor for the intensity nor for the direction. Similar stress appears in all the models with retainer immediately for apical of the ferrule and cannot are responsible for eventual root fracture.

The Fig. 7 represents a perspective view of the distribution of the MPS in the cement between the retainer and dentin. The results obtained with models T2H1, T0H0 and T1H1 presented a similar pattern of stress distribution in cement below the ferrula, but different from the model T1H2, which shows higher tensile stresses (up to 4 MPa), which by direction (Fig. 6) suggests greater tendency to loosen or break the cement layer in the region, because the stresses are significantly higher, but the failure of the cement seems unlikely when comparing the absolute values of stress with the stress required to the cement cohesive failure (8.3 MPa).

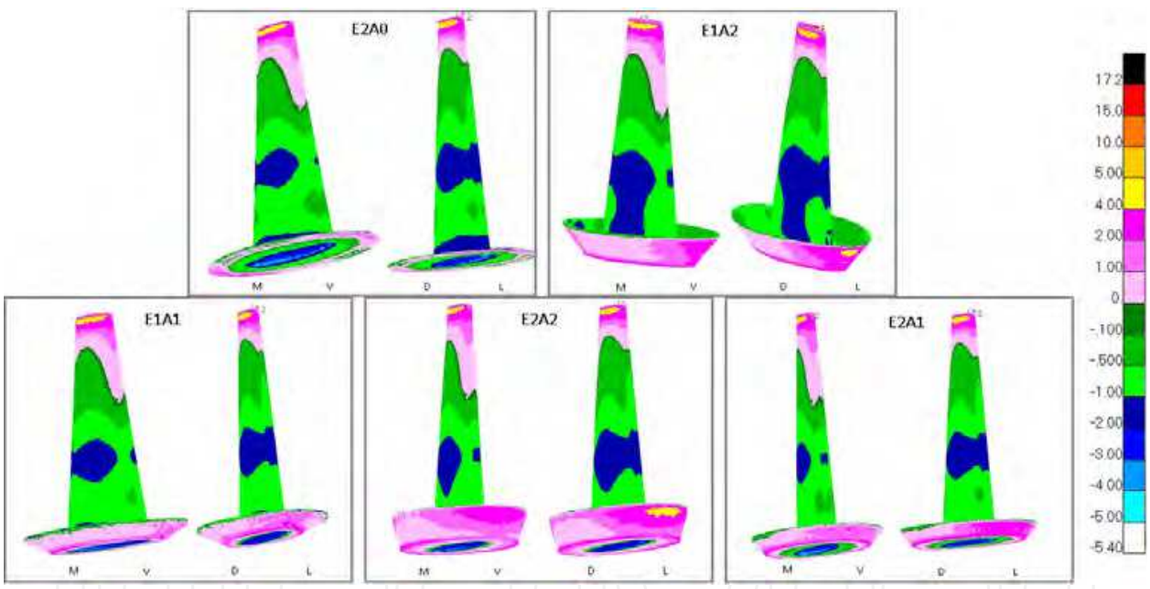

Fig. 7. Perspective view of the cement between the retainer and dentin, MPS in the wedge effect.

3.2 Vestibular lever effect

Under load with inclination of 45º in the vestibular cusp the T2H2, T0H0 and H models answered equally (Fig. 8), except in the radicular dentin that is being doubled and it is observed compressive stress in the vestibular, concentrated in the contact area with the cortical bone that acts as fulcrum (Fig. 9). The tensile stress concentrates and reaches the maximum on the opposite side, lingual, but, unexpectedly, it presents a larger extension in the model with ferrule, with maximum of 104, 110 and 109 MPa for H, T0H0 and T2H2 models, respectively.

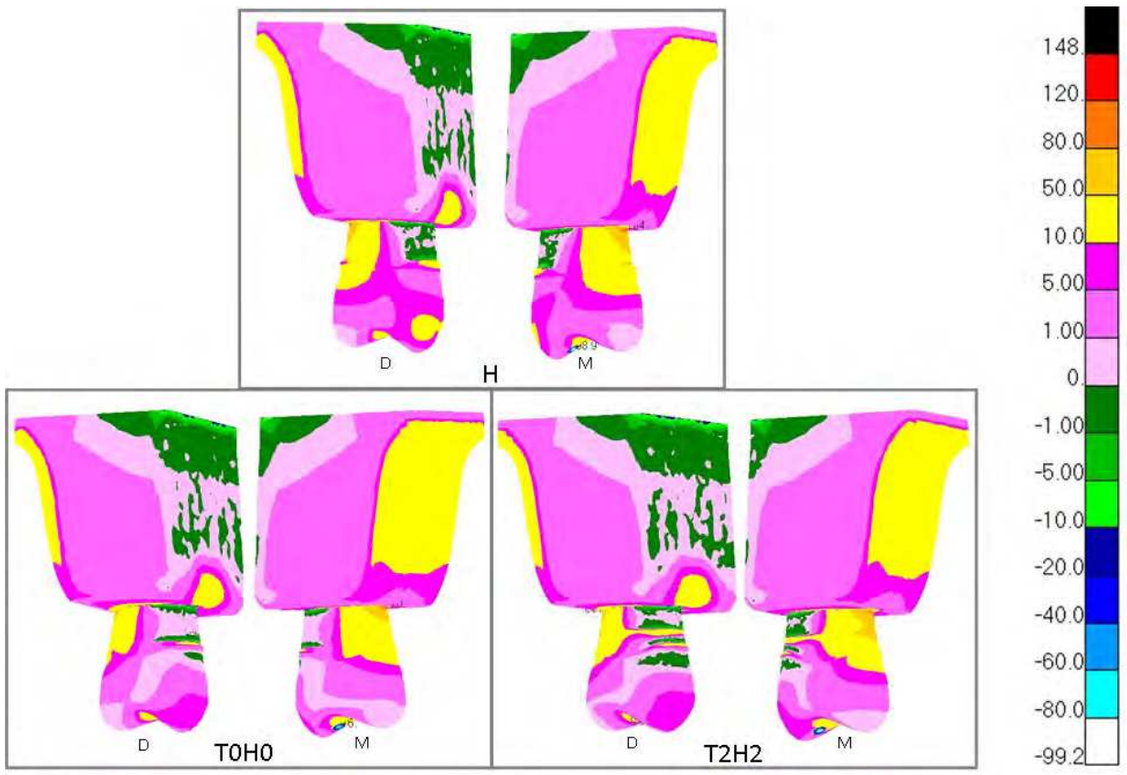

Fig. 8. Perspective view of all structures, MPS in the vestibular lever effect.

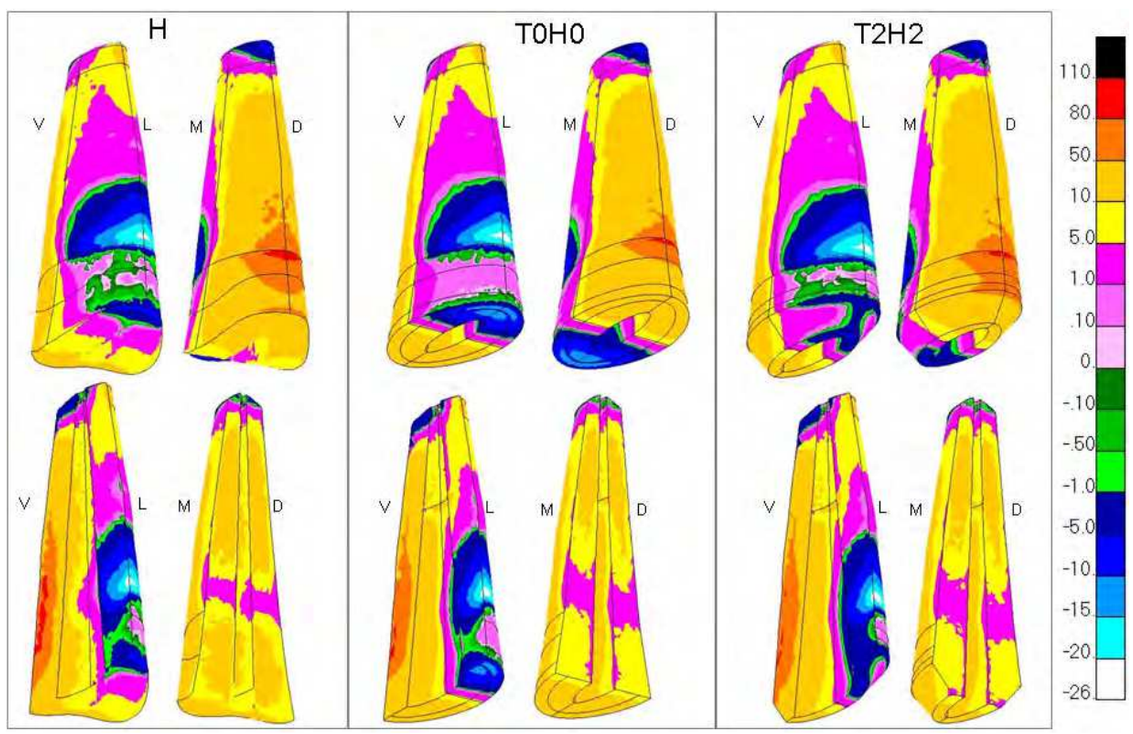

Fig. 9. Perspective view of the dentin, MPS in the vestibular lever effect.

The Fig. 11 represents a perspective view of the distribution of the MPS in the cement between the retainer and dentin and the Fig. 10 shows the MPS vectors in the internal and external surfaces of the radicular dentine at the intersections with in M-D and V-L planes.

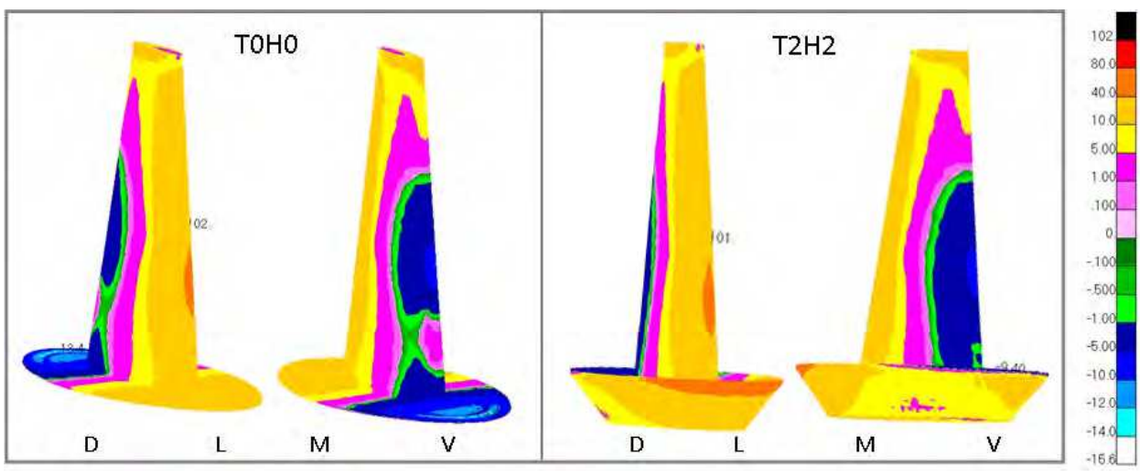

Fig. 10. Perspective view of the cement between the retainer and dentin, MPS in the vestibular lever effect.

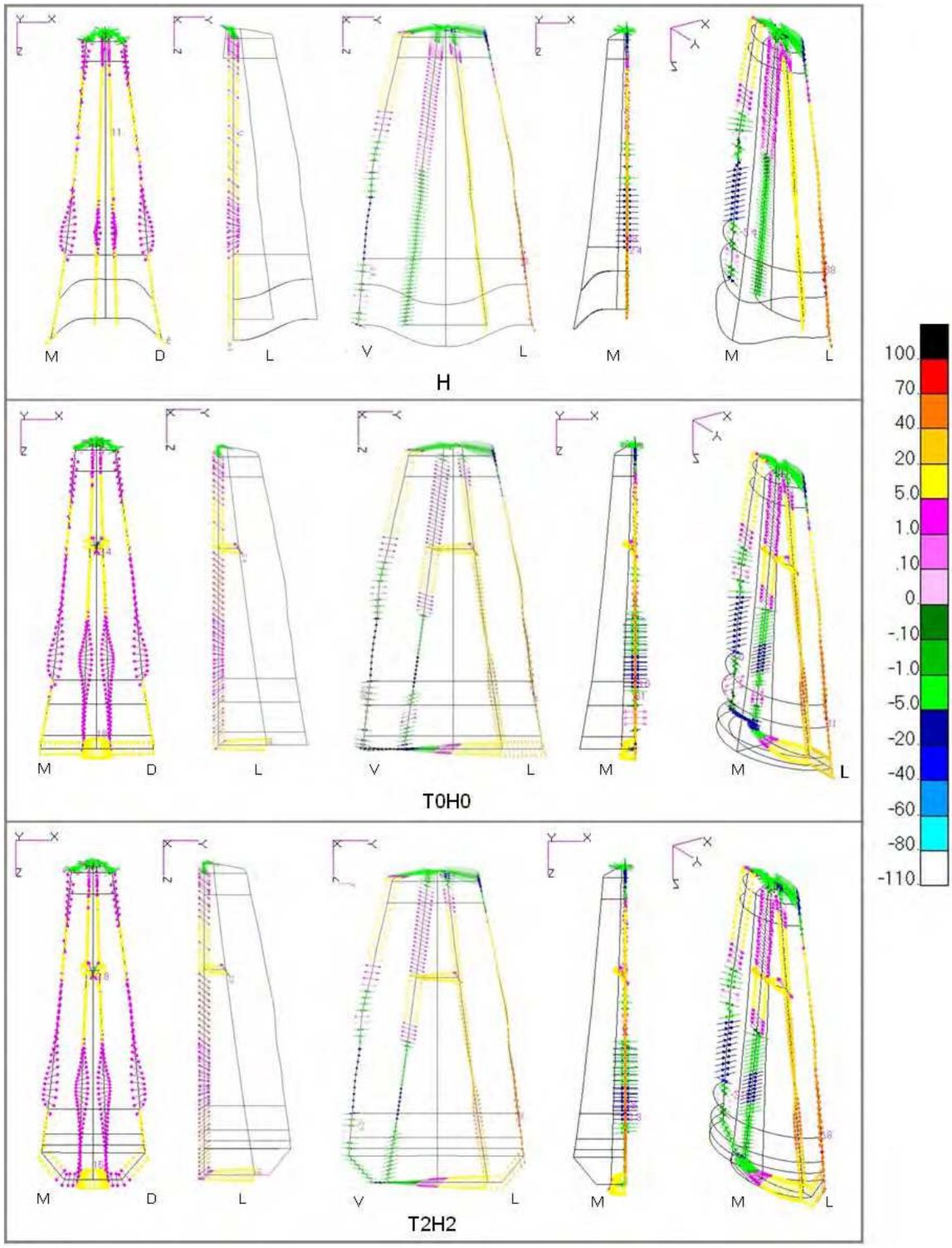

Fig. 11. MPS vectors in the surfaces of the radicular dentine in the vestibular lever effect in M-D and V-L slices.

3.3 Proximal lever effect

The Fig. 12 shows the results under load parallel to the tooth's long axis in the mesial marginal ridge. The maximum tensile stress in dentin (Fig. 13) at the distal edge are also much seemed (68, 68 and 67 MPa), smaller than in the vestibular lever effect.

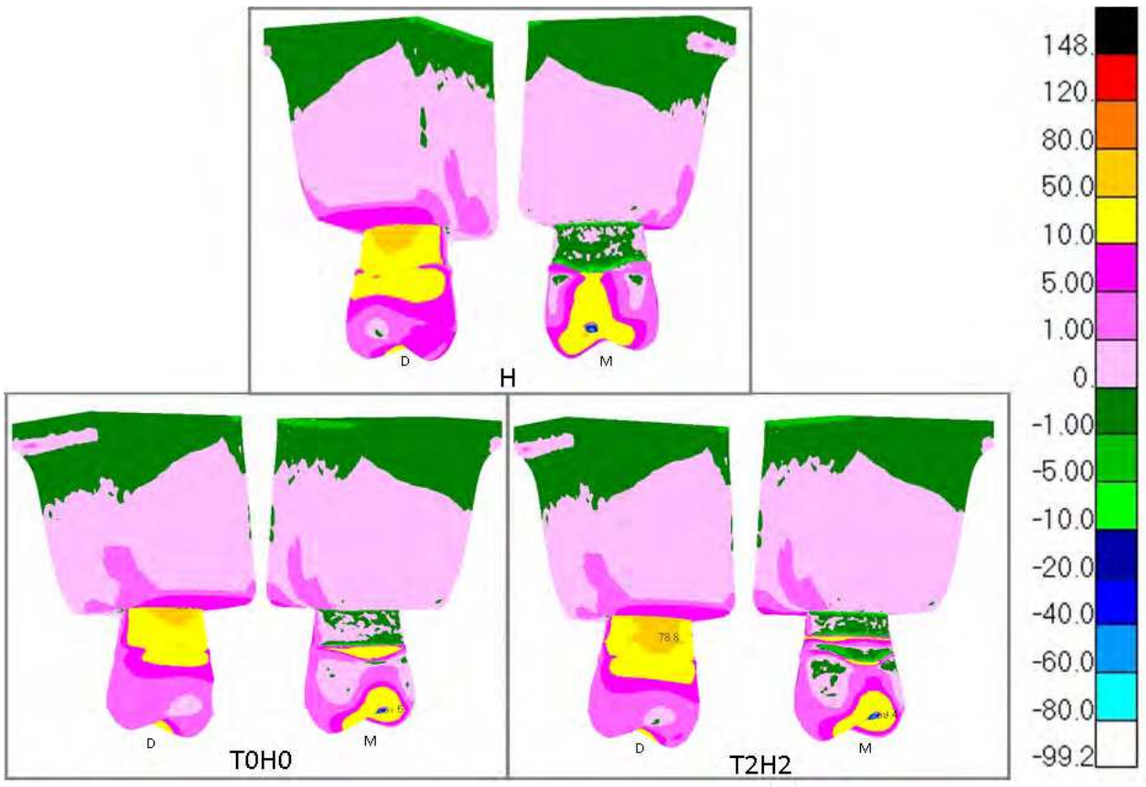

Fig. 12. Perspective view of all structures, MPS in the proximal lever effect.

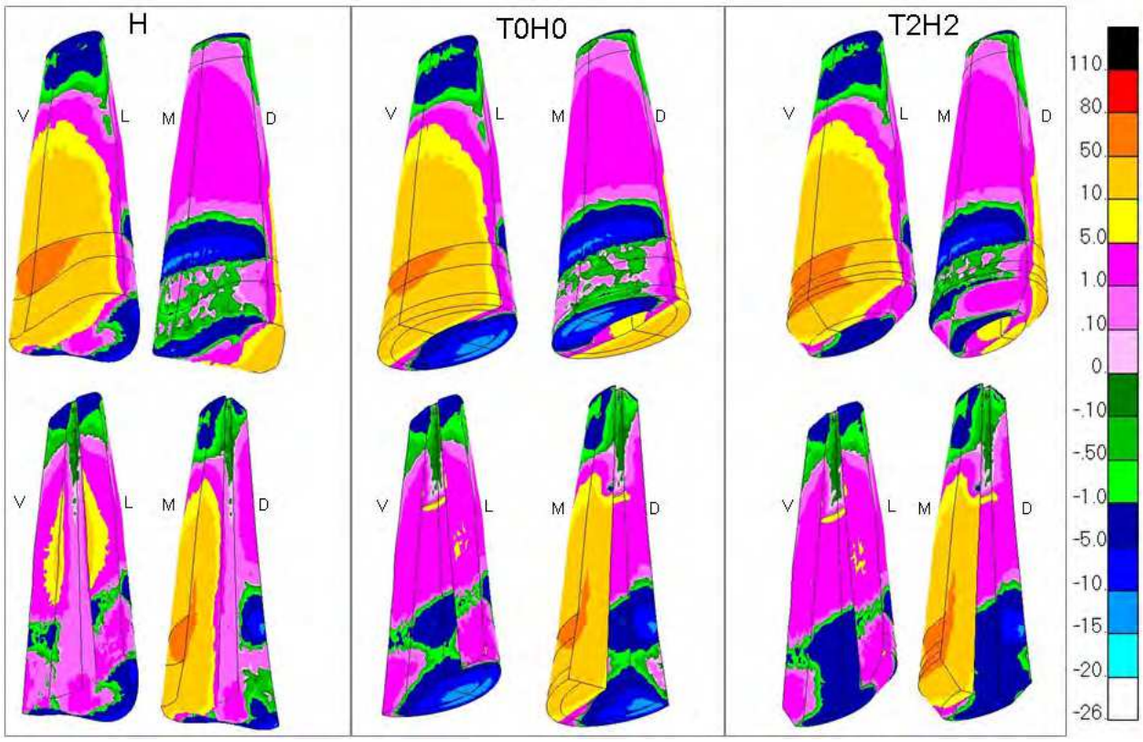

Fig. 13. Perspective view of the dentin, MPS in the proximal lever effect.

The Fig. 14 represents a perspective view of the distribution of the MPS in the cement between the retainer and dentin and the Fig.15 shows the MPS vectors in the internal and external surfaces of the radicular dentine at the intersections with in M-D and V-L planes. The stress orientation in all of the cases is similar.

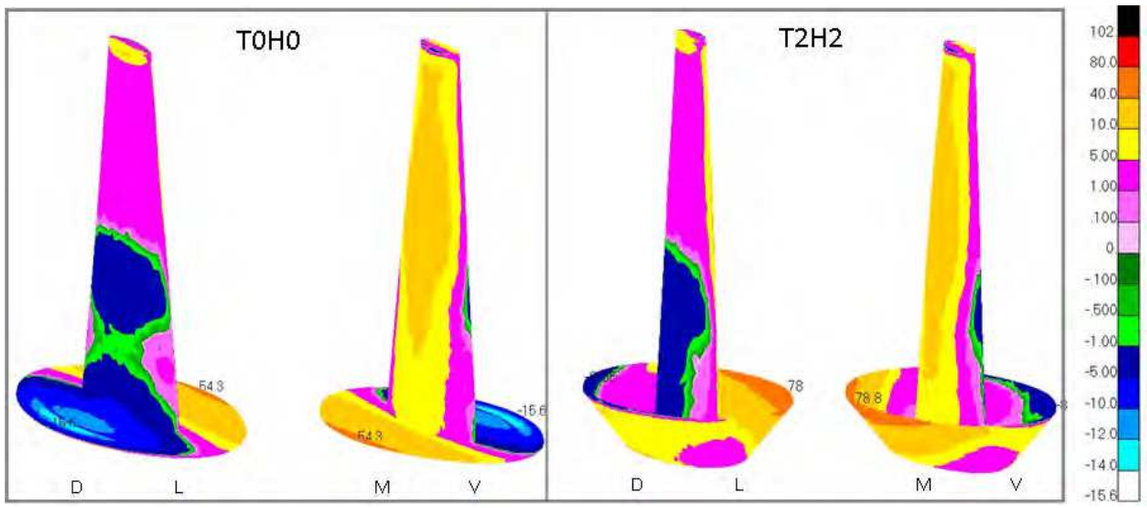

Fig. 14. Perspective view of the cement between the retainer and dentin, MPS in the proximal lever effect.

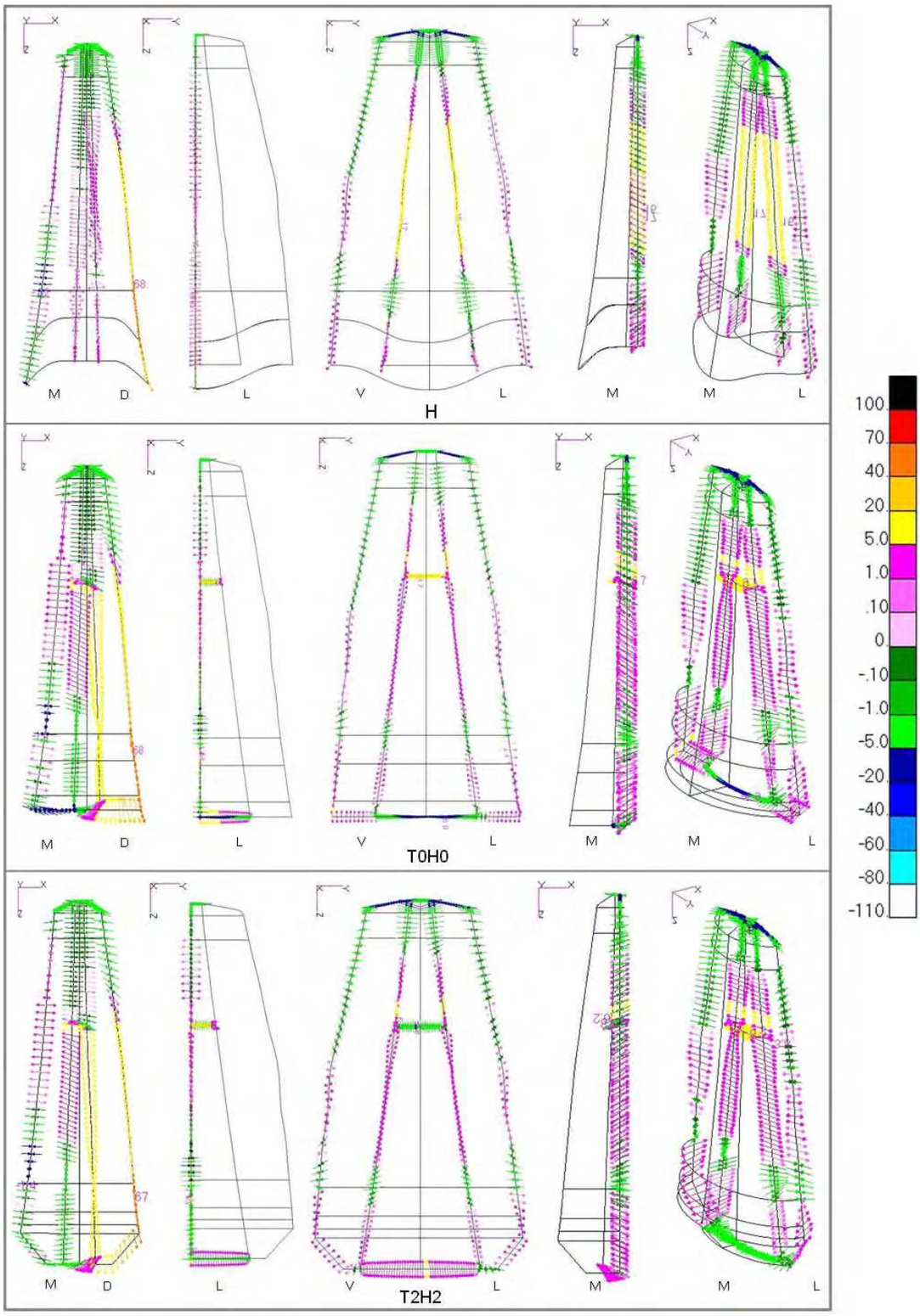

Fig. 15. MPS vectors in the surfaces of the radicular dentine in the proximal lever effect in M-D and V-L slices.

3.4 Torsion effect

The Fig. 16 shows the MPS results in all structures under oblique load with 45º in relation to the tooth's long axis pointed to vestibular cusp in the mesial marginal ridge.

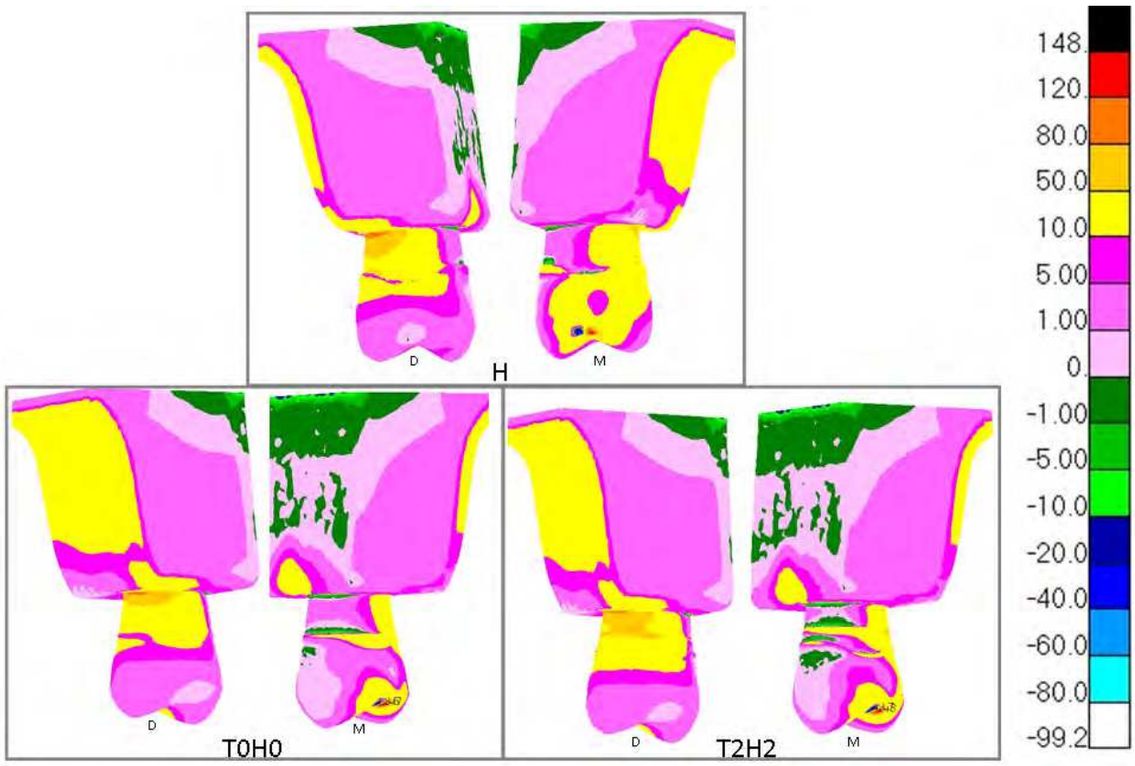

Fig. 16. Perspective view of all structures, MPS in the torsion effect.

The MPS in dentin are present in Fig. 17. The Fig. 18 represents a perspective view of the distribution of the MPS in the cement between the retainer and dentin and the Fig.19 shows the MPS vectors in the internal and external surfaces of the radicular dentine at the intersections with in M-D and V-L planes.

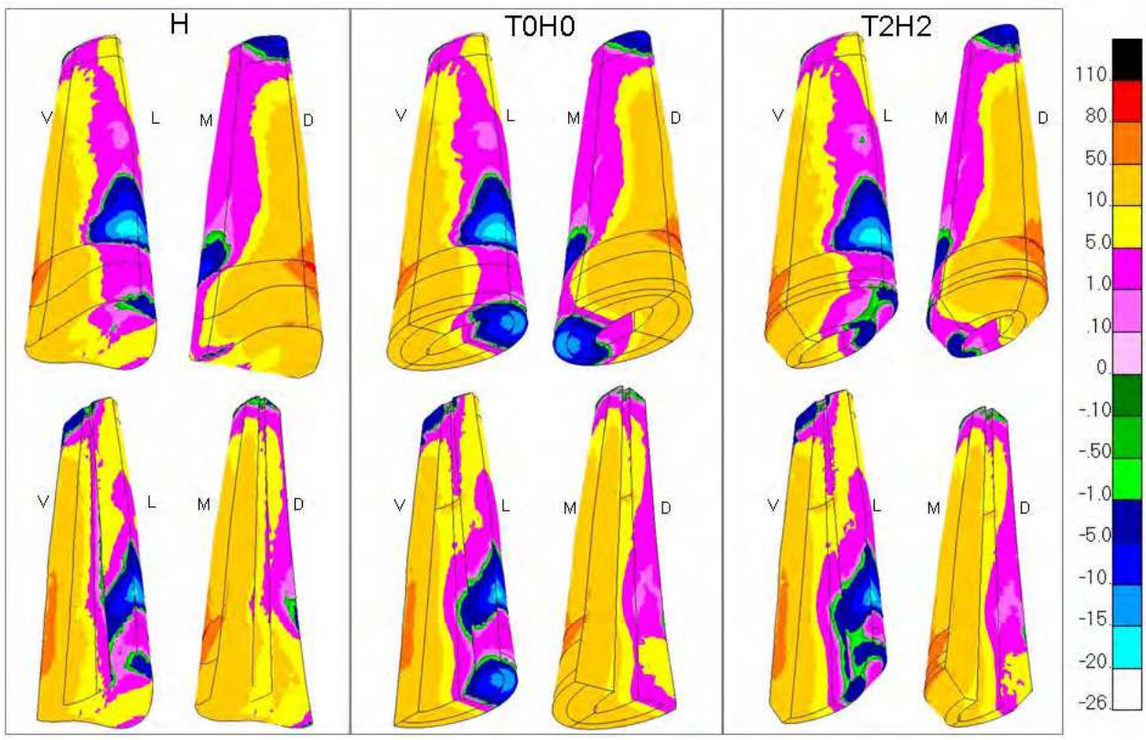

Fig. 17. Perspective view of the dentin, MPS in the torsion effect.

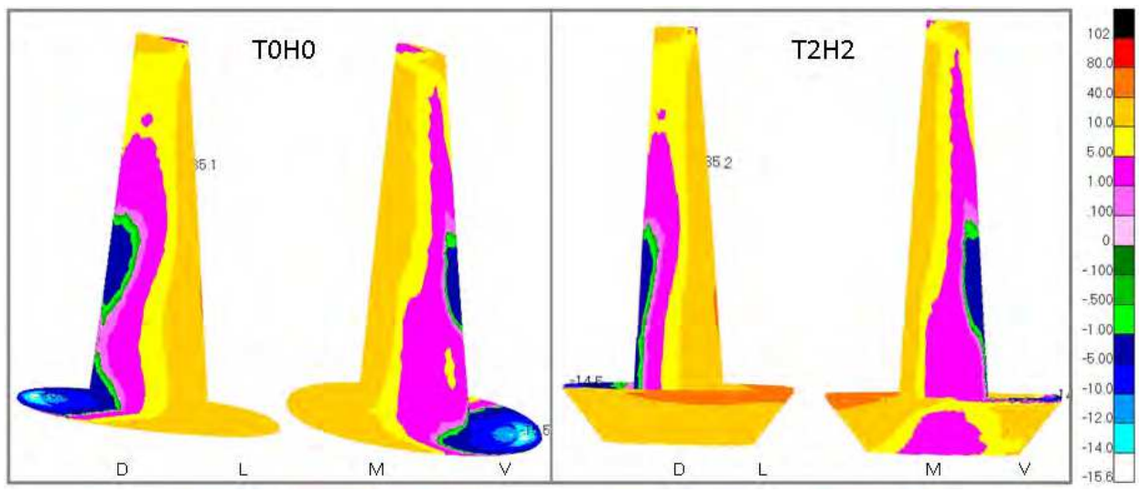

Fig. 18. Perspective view of the cement between the retainer and dentin, MPS in the torsion effect.

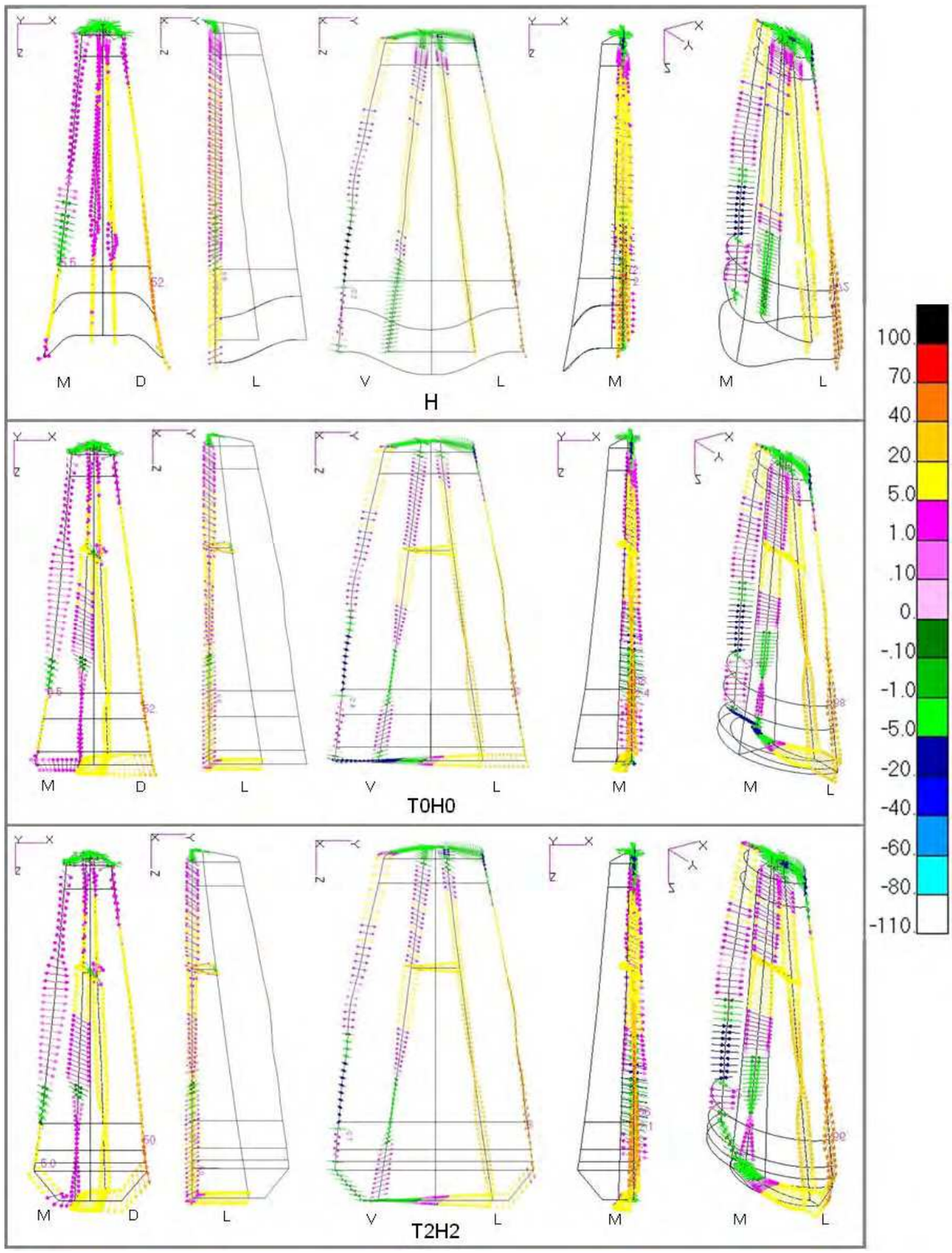

Fig. 19. MPS vectors in the surfaces of the radicular dentine in the torsion effect in M-D and V-L slices.

3.5 Stress plot in wedge, vestibular lever, proximal lever and torsion effect

The Figs 20 to 28 shows the MPS in a ridge A to B, indicated in the drawing corresponding to each graph, in the surface of root dentin (interface with periodontal ligament), depending on the relative position of the node under every load, due to the abcissa axis is adimensional (Distance/Total length),.

The Fig. 20 shows the outside edge of the lingual surface. It is observed that the models that generate the wedge or proximal lever present in the lingual edge, very low stresses, all of the same order of magnitude. Since the models that generate vestibular lever and torsion have high tensile stresses in this edge, but below the dentin´s strenght limit.

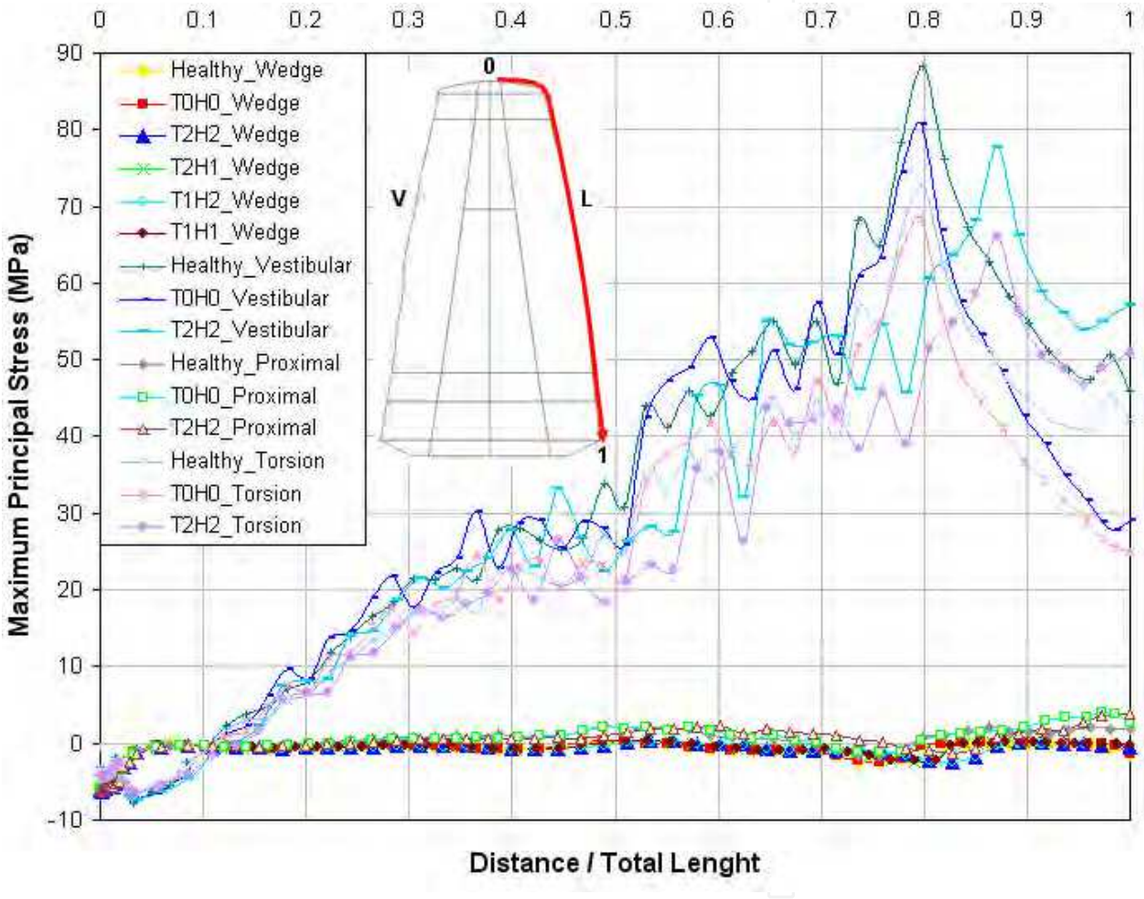

Fig. 20. MPS at the edge of the root dentin on the lingual surface, from the apex to the cervical direction.

The Fig. 21 shows the outside edge of the vestibular surface. It is observed that the models that generate proximal wedge and proximal lever have the same order of magnitude of stresses acting on the vestibular edge with inflection behavior (tensile to compressive) from the apex to the cervical direction. In models that generate proximal lever, the tensile stresses near the apex are close to the wedge effect, however, near the neck, the stress tensile increase up to 5 MPa.

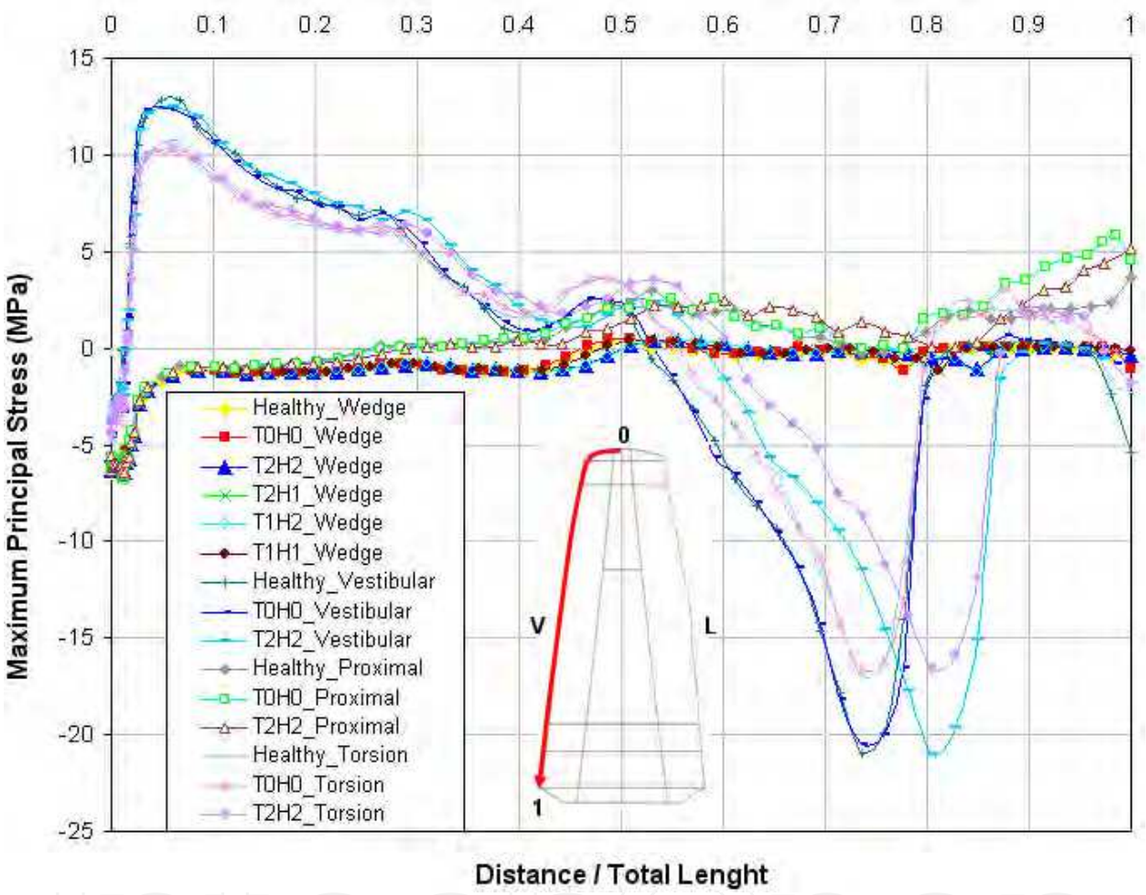

Fig. 21. MPS at the edge of the root dentin on the vestibular surface, from the apex to the cervical direction.

The Fig. 22 shows the outside edge of the distal surface. We observed lowest stresses in wedge models, followed by vestibular lever models, torsion models and reaching the maximum stresses in proximal lever models. In models of proximal lever and torsion effect are generated stress peaks on the same nodes of the same models; the lower stress in torsion models could be due to the lower longitudinal component of the load in this case.

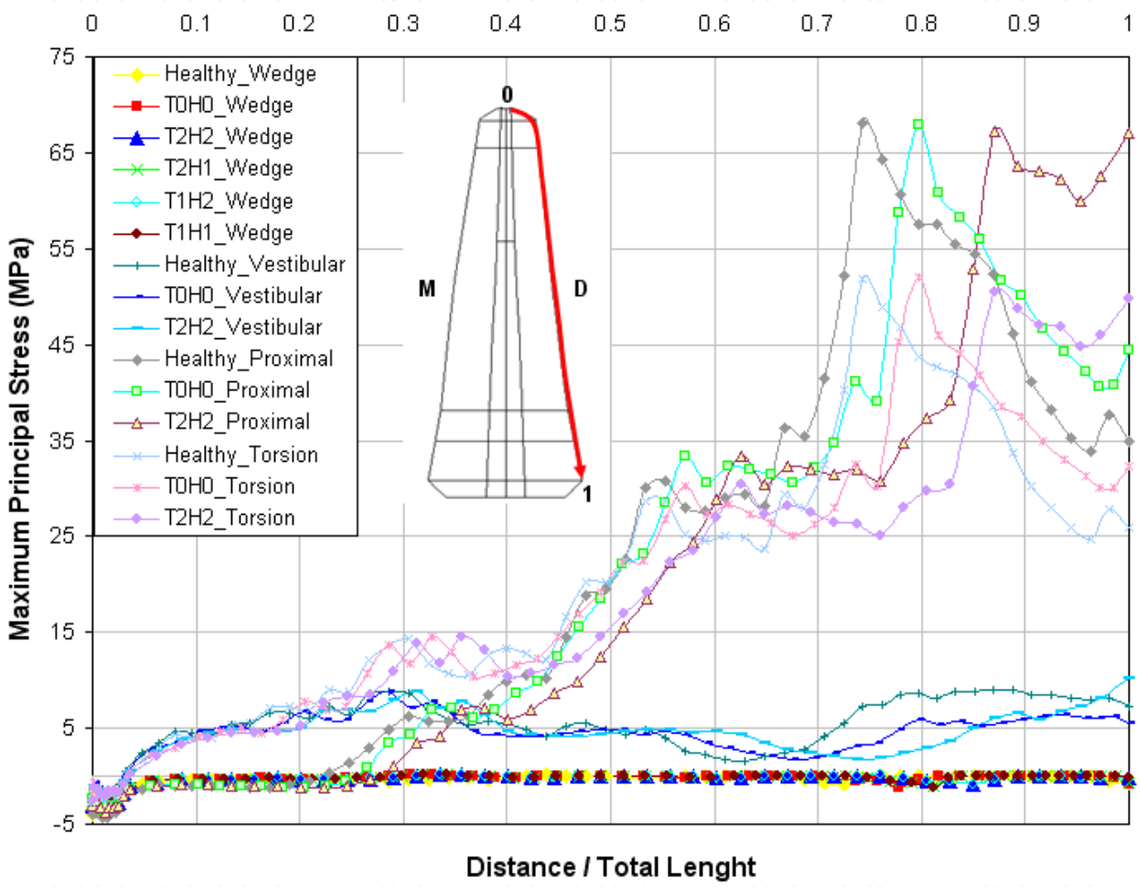

Fig. 22. MPS at the edge of the root dentin, the distal surface, from the apex to the cervical, under all loads

The Fig. 23 shows the outside edge of the mesial surface. We observed lowest stresses in wedge models. The inversion of tensile to compression stress occurs so evident in the proximal lever models and so milder in torsion models.

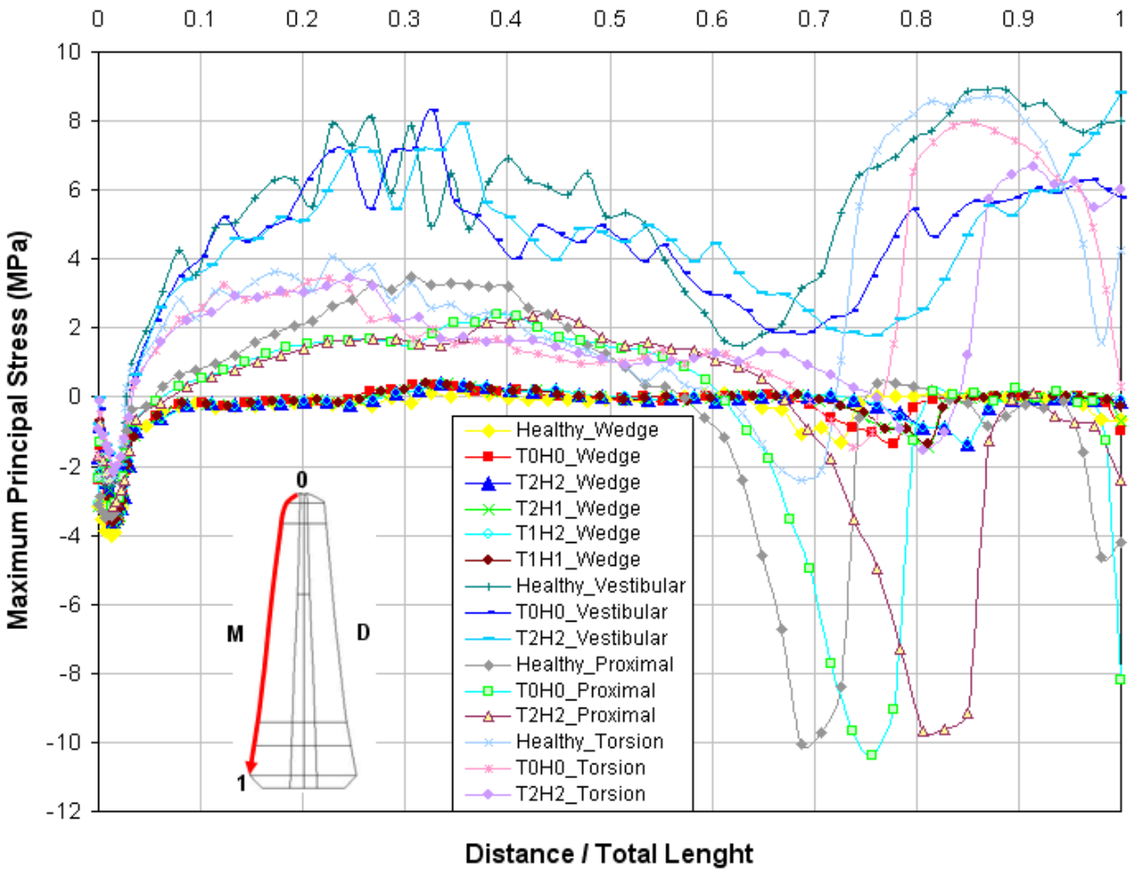

Fig. 23. MPS at the edge of the root dentin in the mesial side, from the apex to the cervical, under all loads.

The Fig. 24 shows the inner edge of the lingual surface. We observed lowest stresses in the models of wedge and tensile stresses up to 45 MPa in the models of vestibular lever, followed by models of torsion effect, but in both types of load, in models of healthy tooth the stresses are smaller. It seems important to note that the order of values is much lower than those in Fig. 20, corresponding to the outer surface, which leads to think that the fracture is expected to start on the outside, apparently motivated by folding of the tooth as a whole. Discard the possibility of fracture driven by stress concentration on the inside face, which could be motivated by the wedging effect promoted by the retainer.

The Fig. 20 shows that the highest stress on the outside edge was achieved by the healthy tooth model. However, it is unlikely that the healthy tooth had a greater tendency to fracture: this is not what is observed in practice.

On the other hand Fig. 24 shows the stress almost doubles in inner edge, for the cases of vestibular lever with retainer, compared to the healthy tooth. This suggests that the failure criterion should not be simply the value of the maximum principal stress, but must be influenced by the stress gradient.

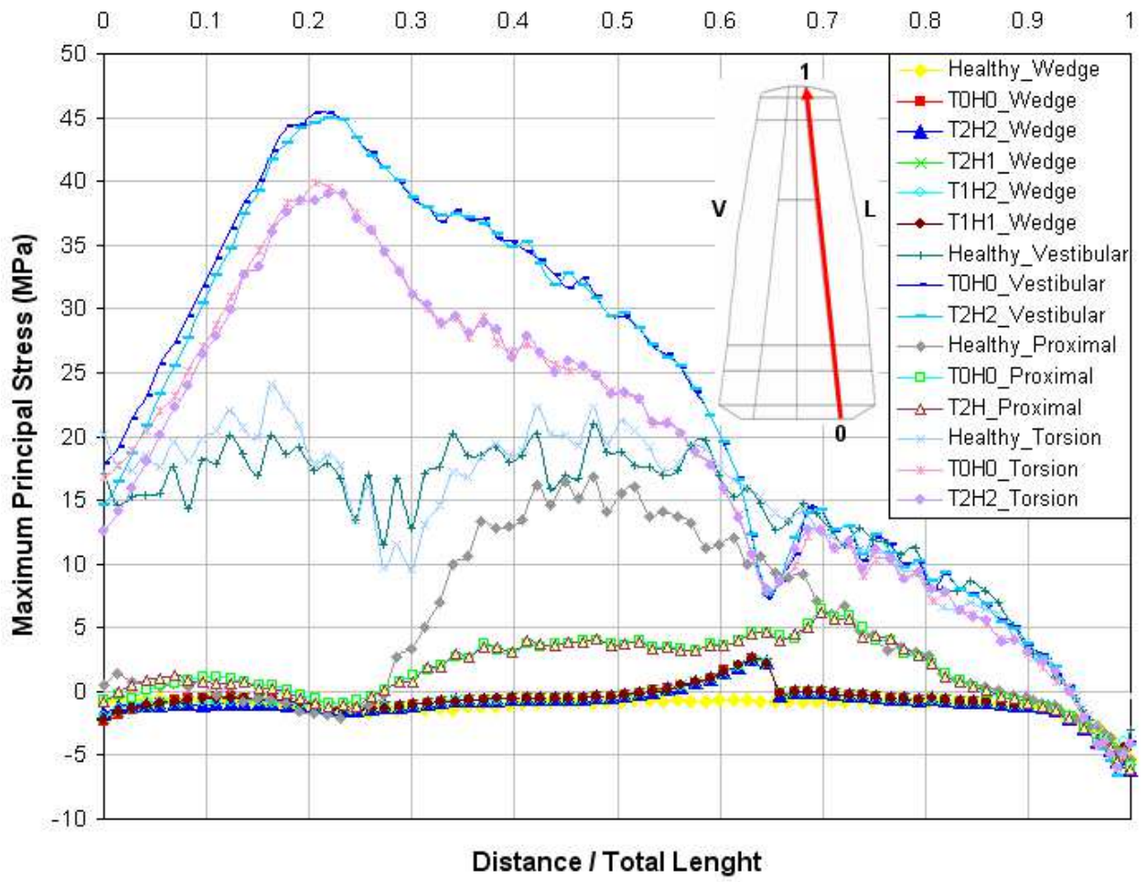

Fig. 24. MPS at the edge of the root dentin on the lingual surface, from the apex to the cervical, under all loads

The Fig. 25 shows the inner edge of the vestibular surface. Tensile stresses are observed up to 27 MPa in the region near the retainer apex in the models that generate vestibular lever, followed by models that generate torsion, but in both types of loading, the stresses are smaller in the healthy tooth models. Figure 11 shows that the direction of the peak tensile is radial and therefore not likely to cause longitudinal fracture but delamination in the dentin and detachment of the retainer apex. In fact, presents a direction parallel to the tensile stress on the edge of the external vestibular root, which appears to be motivated by the apical ligament region, to oppose the rotation of the tooth that is supported by the vestibular cortical bone.

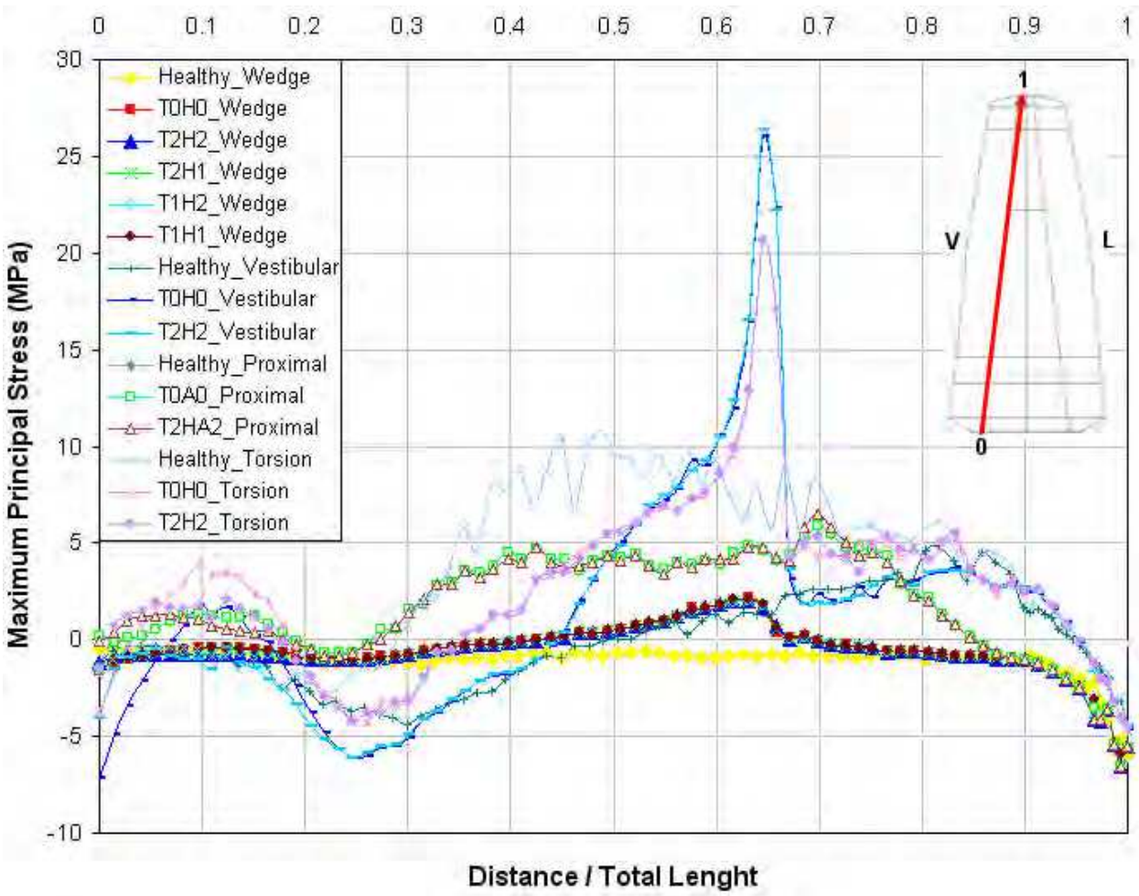

Fig. 25. MPS at the edge of the root dentin on the vestibular surface, from the apex to the cervical, under all loads

The Fig. 26 shows the inner edge of the distal surface. We observed lowest stresses in wedge models. Except the loading wedge models, all have tensile stresses, which shows that practically the entire thickness of the wall works in traction. Moreover, none of the models exceeded the stress developed by the model of healthy tooth with proximal lever load, which leads to the hypothesis that in no case has reached the stress level compatible with the fracture.

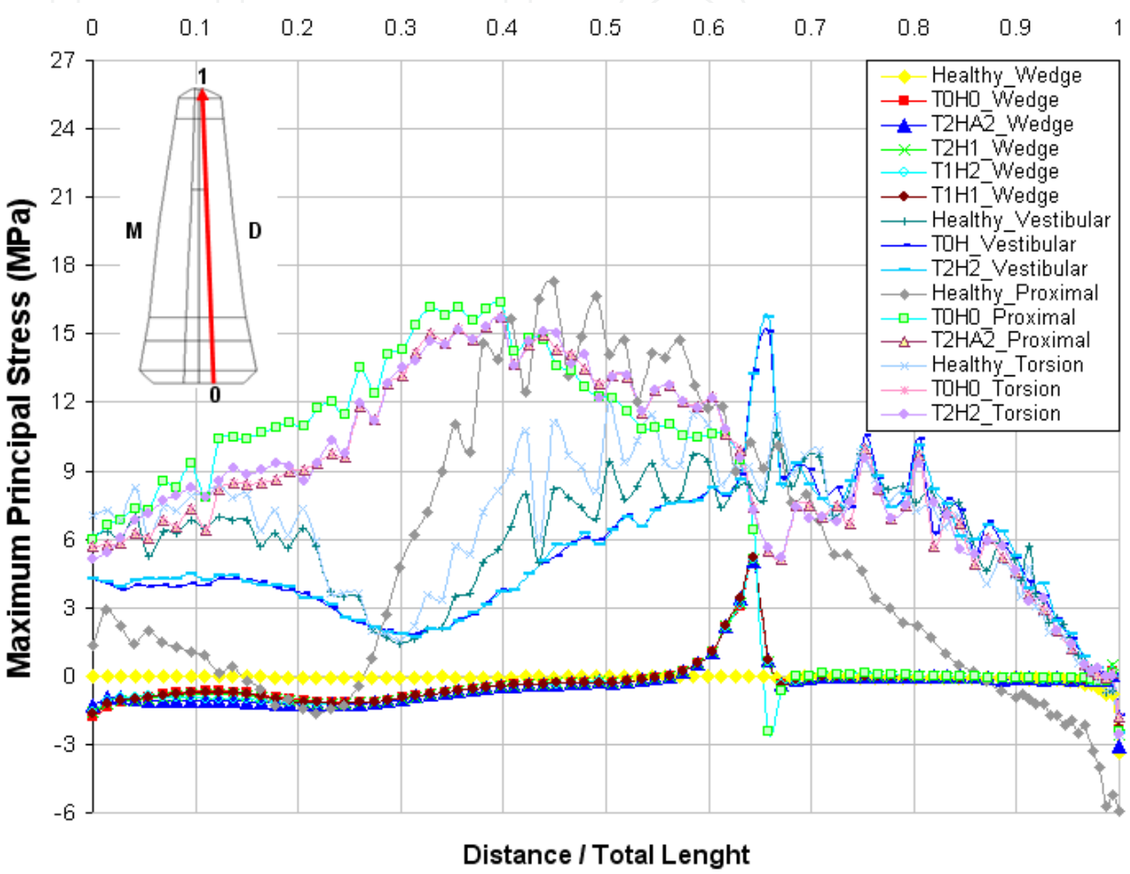

Fig. 26. MPS at the edge of the root dentin, the distal surface, from the apex to the cervical, under all loads.

The Fig. 27 shows the inner edge of the mesial surface. We observed lowest stresses in wedge models. The highest tensile stress occur to the torsion effect, regardless of the presence or not of the ferrula, which also does not help to reduce the stress on the lever vestibular.

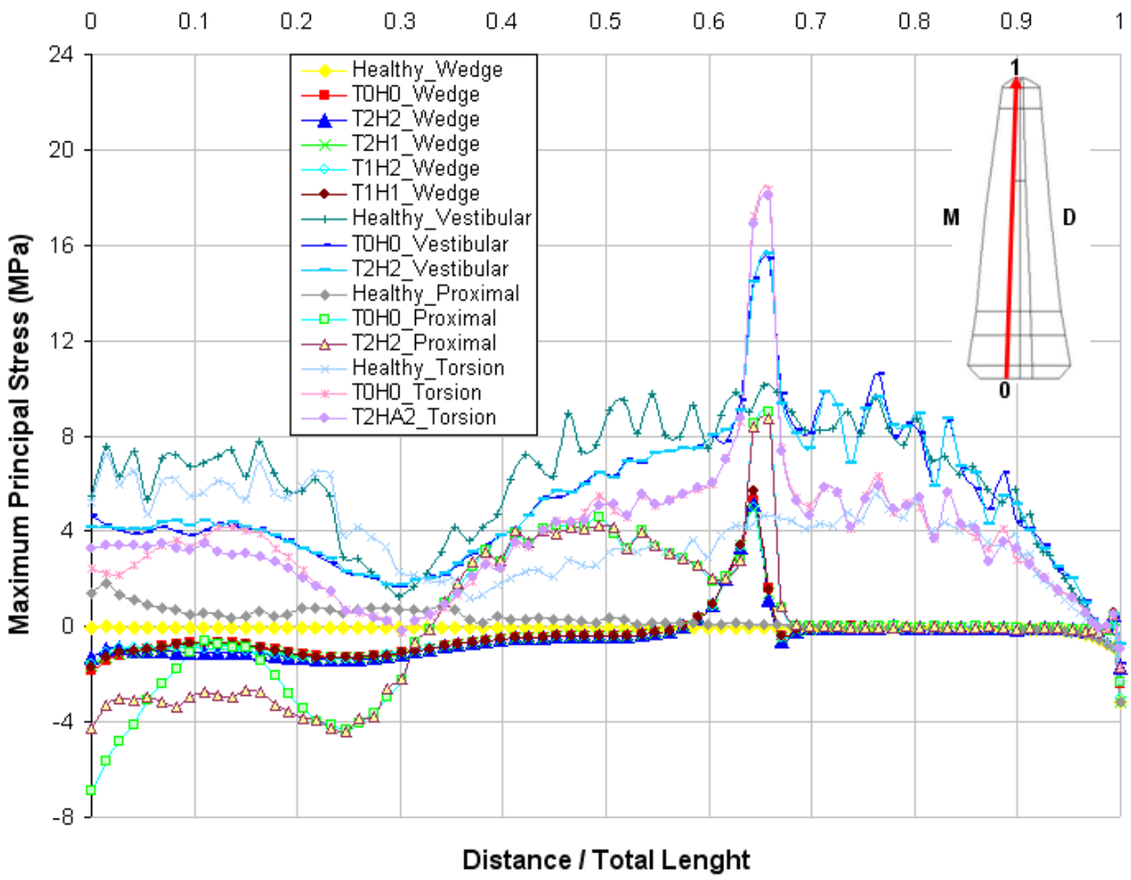

Fig. 27. MPS at the edge of the root dentin in the mesial side, from the apex to the cervical, under all loads.

In Figure 28 shows the circular edge of the inner dentin around the apex of the retainer. The abscissa axis is adimensional (Distance/Total length), where the 0 and 1 represents the vestibular, 0.25 the mesial, 0.5 the lingual and 0.75 the distal aspect. We observed lowest stresses in wedge models, followed by models of proximal lever, torsion and vestibular lever models. The region that remains the most tensioned is the vestibular.

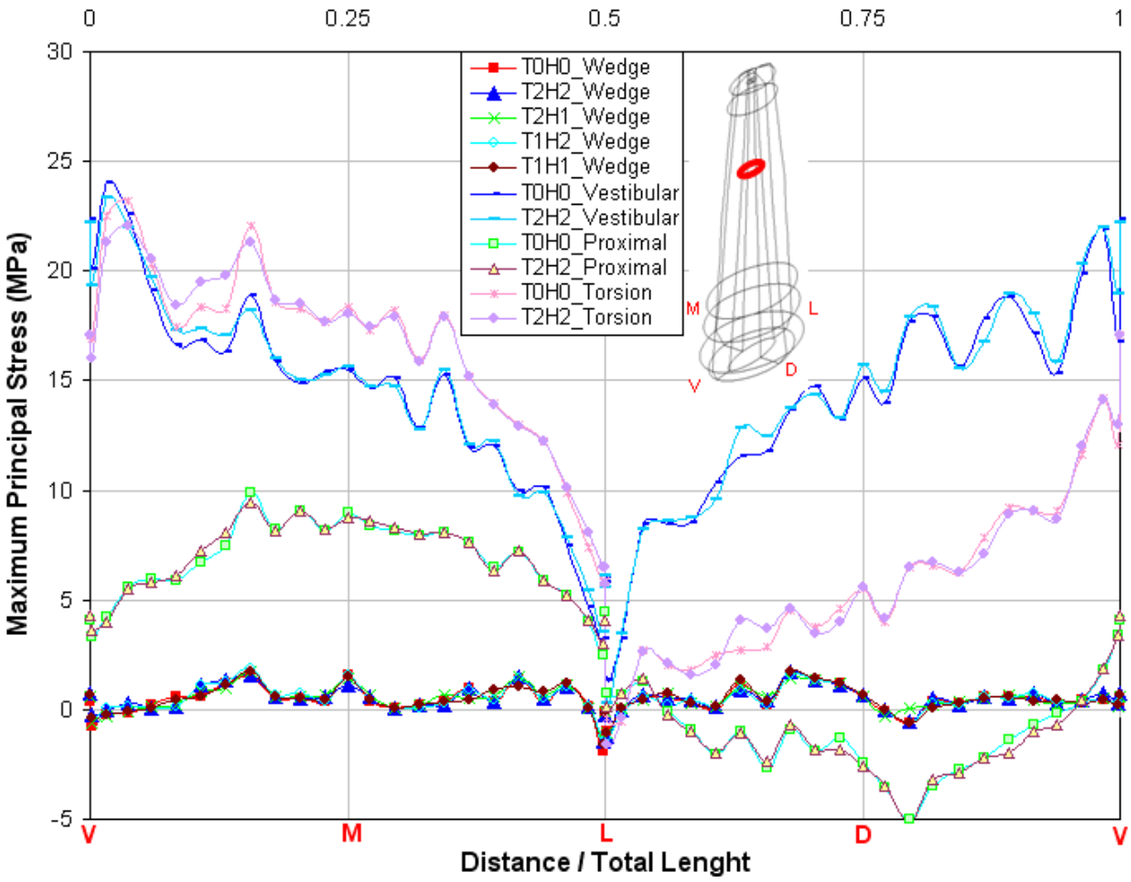

Fig. 28. MPS shown in the circular edge of the inner dentin (VMLDV) around the apex of the retainer under all loads.

4. Discussion

Several studies (Pierrisnard et al., 2002; Zhi-Yue & Yu-Xing, 2003) show that the ferrule creates a positive effect in the reduction of the stress concentration in the dentin-core junction and helps to maintain the integrity of the cement seal in the crown (Libman & Nicholls 1995).

However, in spite of some authors recommend a coronary minimum height of ferrule (Tan et al., 2005; Pereira et al., 2006; Morgano, 1996; Morgano & Bracket, 1999; Aykent, 2006) to increase the fracture strength values, in this study the ferrule didn't influence on the stress distribution. An important observation should be made: for the perfect adhesion among the structures, it was not possible to notice a wedge effect appreciable.

Under load with parallel resultant to the long axis, all of the models present compression stress in the root apex, but with very low intensity when compared with the compression strength of dentin. The light stress concentration found around of the post apex cannot are responsible by longitudinal fracture, because the orientation and the intensity would not justify the fracture.

The results of models T1H1 and T2H1 show that the increase in the width of ferrule, keeping the height, it was important to the root protection with the ferrule effect, because the compressive stress increased four times. The model T2H2 presented compressive stress in the radicular dentin on the ferrule (0.5 to 2.0 MPa) and in the radicular dentin above the periodontal ligament (0.5 to 20 MPa), mesial and distal face (Fig. 4).

On the other hand, the results of models T1H2 and T2H2 show that tensile stresses disappears in the dentine in contact with the ferrule, what can be attributed to the increase in the ferrule width, keeping the height. This characteristic confers to the ferrule design some superiority, because it can be inferred that it will be more difficult than the cement is unstuck in that area, since the tensile stress isn't submitted. The model T2H2 seems also to minimize the tensile stress in the cervical dentine (compressive stress from 0.5 to 2.0 MPa) and in the radicular dentine near to the periodontal ligament, following by the model T2H1, T1H1 and T1H2.

Posteriors teeth can be subject also to vestibular lever effects whenever requested eccentric efforts in lateral excursion. The contact oclusal on the work side in lateral excursion can reach the vestibular cusp in posteriors teeth, generating lever force on the involved roots that serve as guide for those movements.

Under load with inclination of 45º in the vestibular cusp, the maximum stress value is compatible with the fracture occurrence. If the fracture begins at that place can follow a perpendicular plan to the tensile vector and to spread tending the uprighting that suggests a vertical radicular fracture would pass exactly in the bone crest limit.

Fractures vertical appear as a result of stresses generated inside the root canal (Lertchirakarn et al., 2003), but the models showed tensile stress concentrated in the post apex, although of smaller magnitude that in the height of the bone crest.

In all of the models, the root canal stress in the mesial-distal slice presented tensile stress (except for the area near to the post apex) and near to the bone crest presents change in the vector orientation due to the rotation of the same ones, that it seems related with the presence of cortical bone. Therefore, the fracture area not just depends on the post and ferrule, but also of location of the tooth in the alveolus.

An interesting finding was the relatively small difference among the three models that could be attributed to the fact of the interfaces between the structures of the models was simulated with perfect adhesion. The perfect adhesion can losing in the course of time, what would explain that the failures didn't use to happen in retainer recently cemented. On the other hand, the models showed high tensile stresses concentration in more than half of the cement layer, which could be responsible for cohesive fracture.

Under the load area the tensile stresses on the ferrule generates 40 MPa, exceeding the cement's tensile strength of 8.3 MPa and associated with the stress orientation (Fig. 11) suggests the tendency to the cement layer failure in this area.

Under load parallel to the tooth's long axis in the mesial marginal ridge, the tooth restored with post would present a tendency to the rupture similar to the one of the natural, what is not supported by the clinical observations. The explanation for this discrepancy could be again in the fact that the cement layer presented stresses much larger than the necessary

ones for cohesive fracture. After the cement failure the stress distribution change and could propitiate the root fracture.

The intra-radicular retainers can be subject also to rotation force or torsion, whenever requested clinically through contacts functional cusp in the ridge, in other words, tooth relationship to two teeth (Hemmings et al., 1991).

The occlusal contacts in the marginal ridge of the premolar could produce a torsion loads that tends to rotate the root along the tooth's axis. For this reason is extremely important have in mind the use of retainers that offer larger safety to the radicular remnant in any situation of mechanical effort what the root is submitted.

Under oblique load with 45º in relation to the tooth's long axis pointed to vestibular cusp in the mesial marginal ridge, the maximum stress and orientation evidences again that cement layer is prone to failure and that the stress concentration is more serious in the ferrule case. When the cement around of the most coronary portion deteriorates, the fulcrum migrates to apical, what increases the lever arm progressively (Cohen et al., 1993).

The modeling in this study considered all the components without setting out eventual contact problems, in other words, without cement failure, what couldn't happen in the clinic reality.

Regarding the clinical significance of the results, it seems that the best way to protect the radicular remnant when restored with post would be to guarantee the occlusal adjustment, that don't happen loads different from the longitudinal. The most vulnerable part of the whole restorative system is the cement layer, that doesn't resist to the tensile stresses result from the loads application different from the longitudinal load. The post perfectly adhered doesn't seem lead to the occurrence of longitudinal fracture (below the bone crest), but probably to fracture that would begin in the vestibular in the height of the bone crest.

5. Conclusions

Within the limitations of this study, the following conclusions were drawn:

1. In spite of none of the simulated cases to evidence the wedge effect, the longitudinal load produced stresses that don't justify the rupture nor of the dentine nor of the cement layer and the stresses are very inferior to developed by all the other load types;
2. The ferrule isn't necessary to improve the stresses distribution, except for longitudinal load, in that presents discreet beneficial effect;
3. In the vestibular load were found, in the lingual face, tensile stresses guided parallel to the longitudinal axis and magnitude enough to induce vertical fractures above the bone crest. These stresses are associated to the tooth's bend, leaning in the cortical bone that it acts as a fulcrum;
4. In the cement layer were found stresses that are prone to fracture in all of the loads, except for the case of longitudinal load;
5. A concerted effort to develop other FE models to improve the results may provide more reliable data about the non-linearly of the structures and the cement failures in the clinic reality;
6. The analyses help the field better understand the biomechanical analysis of restored teeth with cast intra-radicular retainer with and without ferrule.

6. Acknowledgements

This study was partially based on a thesis submitted to the University of São Paulo, in fulfillment of the requirements for PhD degree. The authors are grateful to the CAPES (Coordenação de Aperfeicoamento de Pessoal de Nível Superior, Coordination for the Improvement of Higher Education Personnel) that supported this research project.

7. References

Anusavice, JK. (2003). *Phillips' Science of Dental Materials* (11th ed.), Elsevier Science, Saunders.

Assif, D; Gofil, C. (1994). Biomechanical considerations in restoring endodontically treated teeth. *J Prosthet Dent*, Vol. 71, pp. 565-67.

Aykent, F; Kalkan, M; Yucel, MT & Ozyesil, AG. (2006). Effect of dentin bonding and ferrule preparation on the fracture strength of crowned teeth restored with dowels and amalgam cores. *J Prosthet Dent*, Vol. 95, pp. 297-301.

Black, J; Hastings, G. (1998). *Handbook of Biomaterial Properties* (1th ed.), Chapman & Hall, London.

Cantisano, W; Palhares, WR & Santos, HJ. (1987). *Anatomia dental e escultura* (3rd ed.), Guanabara Koogan, Rio de Janeiro.

Cohen, BI; Musikant, BL & Deutsch AS. (1993). Comparison of the retentive properties of two hollow-tube post systems to those of a solid post design. *J Prosthet Dent*, Vol. 70, pp. 234-8.

Cohen, S; Hargreaves, KM. (2005). *Pathways of the pulp* (9th ed.), Mosby, St. Louis.

Farah, J; Craig, R. (1974). Finite element stress analysis of a restored axisymetric first molar. *J Dent Res*, Vol. 53, pp. 859-66.

Ferrari, M; Mannocci, F. (2000). Bonding of an esthetic fiber post into root canal with a 'one-bottle' system: a clinical case. *Int J Endodont*, Vol. 33, pp. 397-400.

Ferrario, VF; Sforza, C; Serrao, G; Dellavia, C & Tartaglia, GM. (2004). Single tooth bite forces in healthy young adults. *J Oral Rehabil*, Vol. 31, pp. 18-22.

Friedman, C; Sandrik, J; Heuer, M & Rapp, G. (1975). Composition and mechanical properties of gutta-percha endodontic points. *J Dent Res*, Vol. 54, pp. 921-25.

Green, D; Brooklyn, NY. (1960). Stereomicroscopic study of 700 root apices of maxillary and mandibular posterior teeth. *Oral Surg Oral Med Oral Pathol*, Vol. 13, pp. 728-33.

Hemmings, KW; King, PA & Setchell, DJ. (1991). Resistance to torsional forces of various posts and core designs. *J Prosthet Dent*, (1991), Vol. 66, pp. 325-9.

Holmes, DC; Diaz-Arnold, AM & Leary JM. (1996). Influence of post dimension on stress distribution in dentin. *J Prosthet Dent*, Vol. 75, pp. 140-7.

Ko, CC; Chu, CS; Chung, HK & Lee, MC. (1992). Effects of post on dentin stress distribution in pulpless teeth. *J Prosthet Dent*, Vol. 68, pp. 421-27.

Kumugai, H; Suzuki, T; Hamada, T; Sondang, P; Fujitani, M & Nikawa, H. (1999). Occlusal force distribution on the dental arch during various levels of clenching. *J Oral Rehabil*, Vol. 26, pp. 932-35.

Lee, SY; Huang, HM & Lin, CY. (2000). In vivo and in vitro natural frequency analysis of periodontal conditions, in innovative method. *J Periodontol*, *Vol.* 71, pp. 632-40.

Lertchirakarn, V; Palamara, JE & Messer HH. (2003). Finite element analysis and strain-gauge studies of vertical root fracture. *J Endod*, Vol. 29, pp. 529-34.

Libman, WJ; Nicholls JI. (1995). Load fatigue of teeth restored with cast posts and cores and complete crowns. *Int J Prosthodont*, Vol. 8, pp. 155-61.

Loney, RW; Kotowicz, WE & McDowel, GC. (1990). Three-dimensional photoelastic stress analysis of the ferrule effect in cast post and cores. *J Prosthet Dent*, Vol. 63, pp. 506-12.

Martinez-Insua, A; Da Silva, L; Rilo, B & Santana, U. (1999). Comparison of the fracture resistances of pulpless teeth restored with a cast post and core or fiber post with a composite core. *J Prosthet Dent,* Vol. 80, pp. 527-32.

Morgano S. (1996). Restoration of pulpless teeth: application of traditional principles in present and future contexts. *J Prosthet Dent*, Vol. 75, pp. 375-80.

Morgano, SM; Bracket SE. (1999). Foundation restoration in fixed prosthodontics: current knowledge and future needs. A literature review. *J Prosthet Dent, Vol.* 82, pp. 643-57.

Pegoretti, A; Fambri, L; Zappini, G & Bianchetti, M. (2002). Finite element analysis of a glass fibre reinforced composite endodontic post. *Biomaterials*, Vol. 23, pp. 2667-82.

Pereira, JR; Ornelas, F; Conti, PCR & Valle, AL. (2006). Effect of a crown ferrule on the fracture resistance of endodontically treated teeth restored with prefabricated posts. *J Prosthet Dent*, Vol. 95, pp. 50-4.

Peyton, FA; Craig, RG. (1963). Current evaluation of plastics in crown and bridge prosthesis. *J Prosthet Dent*, Vol. 13, pp. 743-53.

Pierrisnard, L; Bohin, F; Renault, P & Barquins M. (2002). Corono-radicular reconstruction of pulpless teeth: a mechanical study using finite element analysis. *J Prosthet Dent*, Vol. 88, pp. 442-8.

Poiate, IAVP; Vasconcellos, AB; Andueza, A; Pola, IRV & Poiate Jr, E. (2008). Three dimensional finite element analyses of oral structures by computerized tomograghy. *J Biosc Bioeng*, Vol. 106, No. 6, pp. 906-9.

Poiate, IAVP; Vasconcellos, AB; Santana, RB &, Poiate Jr, E. (2009a). Three-Dimensional Stress Distribution in the Human Periodontal Ligament in Masticatory, Parafunctional, and Trauma Loads: Finite Element Analysis. *J Periodontology*, Vol. 80, pp. 1859-1867.

Poiate, IAVP; Vasconcellos, AB; Poiate Jr, E & Dias KRC. (2009b). Stress distribution in the cervical region in a 3D FE. Brazilian Oral Research, Vol. 23, pp. 161-168.

Poiate, IAVP; Vasconcellos, AB; Mori, M &, Poiate Jr, E. (2011). 2D and 3D finite element analysis of central incisor generated by computerized tomography. *Comput Methods Programs Biomed*, Vol 104, No. 2, pp. 292-9.

Powers, M; Farah, JW & Craig RG (1976). Modulus of elasticity and strength properties of dental cements. *J Am Dent Assoc*, Vol. 92, no paginated.

Rundquist, BD; Versluis, A. (2006). How does canal taper affect root stresses? *Int Endod J*, Vol. 39, pp. 226-37.

Shillingburg, HT; Kaplan, MJ & Grace, CS. (1972). Tooth dimensions – A comparative study. *J South Calif Dent Assoc*, Vol. 40, pp. 830-9.

Shillingburg, HT; Grace, CS. Thickness of enamel and dentin. *J South Calif Dent Assoc*, Vol. 41, pp. 33-52.

Tan, PLB; Aquilino, SA; Gratton, DG; et al. (2005). In vitro fracture resistance of endodontically treated central incisors with varying ferrule heights and configurations. *J Prosthet Dent*; Vol . 93, pp. 331-6.

Tanaka, M; Naito, T; Yokota, M & Kohno, M. (2003). Finite element analysis of the possible mechanism of cervical lesion formation by occlusal force. *J Oral Rehabil*, Vol. 30, pp. 60-67.

Ueti, H; Todescan, R & Gil, C. (1997). Study of the thickness enamel/dentin in function of age, group of teeth and distance in relation to the external portion of the clinical crown. *Rev Pós-Grad da USP*, Vol 4, pp. 153-9.

Weinstein, AM; Klaawitter, JJ & Cook, SD. (1980). Implant-bone interface characteristics of bioglass dental implants. *J Biomed Mater Res*, Vol. 14, pp. 23-29.

Whitworth, JM; Walls, AWG & Wassell, RW. (2002). Crowns and extra-coronal restorations: Endodontic considerations: the pulp, the root-treated tooth and the crown. *Br Dental J*, 2002, Vol. 192, pp. 315-27.

Yamamoto, M. (1985). *Metal-ceramics: Principles and methods of Makoto Yamamoto* (1st ed.), Quintessence, Chicago.

Zhi-Yue, L; Yu-Xing, Z. (2003). Effects of post-core design and ferrule on fracture resistance of endodontically treated maxillary central incisors. *J Prosthet Dent*, Vol. 89, pp. 368-73.

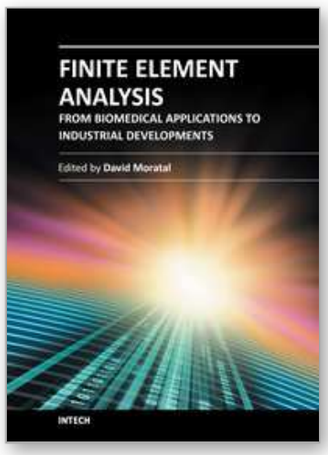

Finite Element Analysis - From Biomedical Applications to Industrial Developments

Edited by Dr. David Moratal

ISBN 978-953-51-0474-2
Hard cover, 496 pages
Publisher InTech
Published online 30, March, 2012
Published in print edition March, 2012

Finite Element Analysis represents a numerical technique for finding approximate solutions to partial differential equations as well as integral equations, permitting the numerical analysis of complex structures based on their material properties. This book presents 20 different chapters in the application of Finite Elements, ranging from Biomedical Engineering to Manufacturing Industry and Industrial Developments. It has been written at a level suitable for use in a graduate course on applications of finite element modelling and analysis (mechanical, civil and biomedical engineering studies, for instance), without excluding its use by researchers or professional engineers interested in the field, seeking to gain a deeper understanding concerning Finite Element Analysis.

InTech Europe
University Campus STeP Ri
Slavka Krautzeka 83/A
51000 Rijeka, Croatia
Phone: +385 (51) 770 447
Fax: +385 (51) 686 166
www.intechopen.com

InTech China
Unit 405, Office Block, Hotel Equatorial Shanghai
No.65, Yan An Road (West), Shanghai, 200040, China
中国上海市延安西路65号上海国际贵都大饭店办公楼405单元
Phone: +86-21-62489820
Fax: +86-21-62489821

IntechOpen